Renewable and Sustainable Energy Reviews 169 (2022) 112851

Contents lists available at ScienceDirect

Renewable and Sustainable Energy Reviews

journal homepage: www.elsevier.com/locate/rser

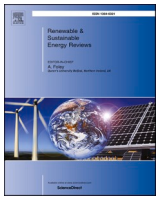

Bioenergy with Carbon Capture and Storage (BECCS) developed by coupling a Pressurised Chemical Looping combustor with a turbo expander: How to optimize plant efficiency

Pietro Bartocci [a,*], Alberto Abad [a], Tobias Mattisson [b], Arturo Cabello [a], Margarita de las Obras Loscertales [a], Teresa Mendiara Negredo [a], Mauro Zampilli [c], Andrea Taiana [d], Angela Serra [d], Inmaculada Arauzo [e,f], Cristobal Cortes [e,f], Liang Wang [g], Øyvind Skreiberg [g], Haiping Yang [h,i], Qing Yang [h,i,j,k], Wang Lu [h], Yingquan Chen [h], Francesco Fantozzi [c,**]

[a] Instituto de Carboquímica (ICB-CSIC), Miguel Luesma Castán 4, 50018, Zaragoza, Spain
[b] Department of Space, Earth and Environment, Division of Energy Technology, Chalmers University of Technology, 10 Gothenburg, SE-412 96, Sweden
[c] Department of Engineering, University of Perugia, Via G. Duranti 67, 06125, Perugia, Italy
[d] Baker Hughes, Piazza Enrico Mattei, 50127, Firenze, Italy
[e] CIRCE Research Institute, University of Zaragoza, Maria de Luna, Zaragoza, 50009, Spain
[f] Department of Mechanical Engineering, University of Zaragoza, Campus Rio Ebro. Building B. Maria de Luna s/n, Zaragoza, 50018, Spain
[g] SINTEF Energy Research, Postboks 4761, Torgarden, Trondheim, Norway
[h] State Key Laboratory of Coal Combustion, Huazhong University of Science and Technology, Wuhan, China
[i] China-EU Institute for Clean and Renewable Energy, Huazhong University of Science and Technology, Wuhan, 430074, China
[j] Department of New Energy Science and Technology, School of Energy and Power Engineering, Huazhong University of Science and Technology, Wuhan, 430074, China
[k] John A, Paulson School of Engineering and Applied Sciences, Harvard University, Cambridge, 02138 MA, United States

ARTICLE INFO

Keywords:
Chemical Looping Combustion
Reaction kinetics
Shrinking core model
Computational Fluid Dynamic
Turbo expanders

ABSTRACT

Carbon Capture and Storage is a technology of paramount importance for the fulfillment of the Sustainable Development Goal 7 (Affordable and Clean Energy) and the Sustainable Development Goal 5 (Climate Action). The European Union is moving rapidly towards low carbon technologies, for instance via the Energy Union Strategy. Coupling biofuels and carbon capture and storage to decarbonize the power and the industrial sector can be done through the development of BECCS (Bioenergy with Carbon Capture and Storage). Chemical Looping combustion is one of the cheapest way to capture CO_2. A Chemical Looping Combustion (CLC) plant can be coupled with a turbo expander to convert energy to power, but it has to work in pressurised conditions. The effect of pressure on the chemical reactions and on fluidised bed hydrodynamics, at the moment, is not completely clear. The aim of this review is to summarize the most important highlights in this field and also provide an original method to optimize power plant efficiency. The main objective of our research is that to design a pressurised Chemical Looping Combustion plant which can be coupled to a turbo expander. To achieve this we need to start from the characteristics of the turbo expander itself (eg. the Turbine Inlet Temperature and the compression ratio) and then design the chemical looping combustor with a top down approach. Once the air and the fuel reactor have been dimensioned and the oxygen carrier inventory and circulation rate have been identified, the paper proposes a final optimization procedure based on two energy balances applied to the two reactors. The results of this work propose an optimization methodology and guidelines to be used for the design of pressurised chemical looping reactors to be coupled with turbo expanders for the production of power with carbon negative emissions.

* Corresponding author.
** Corresponding author.
E-mail addresses: pbartocci@icb.csic.es (P. Bartocci), francesco.fantozzi@unipg.it (F. Fantozzi).

https://doi.org/10.1016/j.rser.2022.112851
Received 31 March 2022; Received in revised form 26 July 2022; Accepted 15 August 2022
Available online 1 October 2022

Nomenclature

Abbreviations

BECCS	Bioenergy with Carbon Capture and Storage
CC	Combined Cycle
CCS	Carbon Capture and Storage
CCU	Carbon Capture and Use
CFD	Computational Fluid Dynamic
CLC	Chemical Looping Combustion
CLC3	Three reactors Chemical Looping Process
CLC-CC	Chemical Looping Combustion Combine Cycle Power Plant
DDPM	Dense Discrete Phase Model
DEM	Discrete Element Method
exCLC	Extended CLC configuration
ECT	Electrical Capacitance Tomography
FB	Fluidised Bed
GT	Gas Turbine
HAT	Humid Air Turbine
ICR	Internally Circulated Reactor
ICR-H_2-2P	ICR plant with an additional combustor and two-phase flow heat exchanger
HRSG	Heat Recovery Steam Generator
KTGF	Kinetic theory of granular flow
MP-PIC	Multiphase Particle-in-Cell Method
NGCC	Natural Gas Combined Cycle
PCLC	Pressurised Chemical Looping Combustion
PCFB	Pressurised Circulated Fluidised Bed
PFB	Pressurised Fluidised Bed
PFIR	Plug-flow Internally-circulating reactor
SCM	Shrinking Core Model
STIG	Steam Injected Gas Turbine
TDH	Transport Disengaging Height
TGA	Thermogravimetric Analyzer
TPM	Two Phase Model

Symbols

b_r	Stoichiometric factor in the reduction reaction
c_g	Specific heat capacity of particles (J/kgK)
c_p	Specific heat capacity of gas (J/kgK)
D	Diameter of the bed (m)
d_b	Average bubble diameter (m)
d_p	Diameter of average bed particles (m)
E_{ch}	Activation Energy for the chemical reaction (kJ mol^{-1})
F_f	Molar flow of the fuel gas (mol/s)
g	Acceleration due to gravity, 9.81 ($m\,s^{-2}$)
G_s	Solid circulation rate ($kg/(m^2\,s)$)
h	Heat transfer coefficient (W/m^2K)
Hd	Vertical distance from the distributor (m)
H_0	Constant
H_f	Expanded height of the bed (m)
h_{gc}	Interphase gas convective component of bed to surface heat transfer coefficient (W/m^2K)
h_{max}	Maximum heat transfer coefficient (W/m^2K)
h_{pc}	Particle convective component of bed to surface heat transfer coefficient (W/m^2K)
h_r	Radiative component of heat transfer coefficient (W/m^2K)
k_0	Pre-exponential factor of the chemical reaction rate constant ($mol^{-1n}m^{3n-2}s^{-1}$)
$k_{0,p}$	Pre-exponential factor of the chemical reaction rate constant at pressurised conditions ($mol^{-1n}m^{3n-2}s^{-1}$)
M	Molecular Mass (g)
m_{ox}	Mass of the oxygen carrier which has been oxidised (Kg)
m_{ox_FR}	Solids inventory of the fuel reactor (Kg)
m_{ox_AR}	Solids inventory of the air reactor (Kg)
m_{red}	Mass of the oxygen carrier which has been reduced (kg)
$\dot{m}_{ox}$	Circulation rate of the oxygen carrier, expressed as the mass of oxygen carrier totally oxidised (Kg/s)
$\dot{m}$	Real circulation rate (Kg/s)
n	Order of reaction
Nu	Nusselt number
P	Operating pressure (MPa)
p	Pressure (bar)
pq	Correlation parameter for kinetics at atmospheric and pressurised conditions
Pr	Prandtl number of gas
$\bar{r}$	Solid reaction rate of the reaction (mol of solid (m^3 of solid)$^{-1}$ s^{-1})
R_0	Oxygen Transport Capacity
U_0	Superficial gas velocity (m/s)
$u_{b\infty}$	Velocity of a single bubble (m/s)
U_g	Superficial gas velocity (m/s)
U_b	Bubble rise velocity (m/s)
U_{br}	Single bubble rise velocity (m/s)
U_j	Jetting gas velocity (m/s)
U_{mf}	Superficial gas velocity at minimum fluidization (m/s)
U_t^{Θ}	Terminal velocity in ambient pressure (m/s)
U_t	Terminal velocity at high pressure (m/s)
u_{tf}	Gas throughflow (m/s)
u_{tr}	Transport velocity (m/s)
u_{vis}	The visible bubble flow (m/s)
x_{NiO}	Mass fraction of NiO in the fully oxidised sample
$X_{S,o}$	Solids conversion in the oxidation reaction

Greek letters

alfa	Equivalence ratio
δ_b	Bubble fraction in the dense bed
ΔXf	Variation in the Conversion rate of fuel
ΔXg	Variation in the Conversion rate of gas
ΔXs	Variation in the Conversion rate of solid
ε	Bed cross-section average voidage
ε_0	Settled bed voidage
ε_{mb}	Minimum bubbling voidage
ε_{mf}	Minimum fluidization voidage
λ_g	Gas thermal conductivity (W/mK)
μ	Gas viscosity (Pa s)
ρ_g	Gas density (kg/m^3)
ρ_p	Solids (particle) density (kg/m^3)
τ	Time for the complete conversion of the solid, for reduction or oxidation reaction (s)
Φ	Characteristic reactivity in the air reactor

1. Introduction

1.1. The GTCLC-NEG power plant concept

In both the Fifth Assessment and the Shared Socioeconomic Pathways reports, the Intergovernmental Panel on Climate Change (IPCC) identifies Bioenergy with Carbon Capture and Storage (BECCS) as a key technology to meet the goal of limiting the increase in the Earth's temperature to less than 2 °C, see Ref. [1]. Nevertheless, BECCS is still under development, and here a highly efficient process could be obtained by coupling bioenergy with chemical looping combustion, see for example the recent work of Mendiara et al. [2] or the work of Ryden

et al. [3]. Many review papers have already dealt with several aspects of chemical looping, see for example [4–9]. There is also a recent interest on pressurised chemical looping as reported in Ref. [10]. Nevertheless, the work on the coupling of PCLC reactors with turbo expanders is still not complete, given that there are many barriers that this process is facing. Here stems the novelty of this paper.

In this context a Marie Curie project has been funded by the European Commission and it is managed by the Spanish National Research Council (CSIC), Instituto de Carboquimica (ICB) in Zaragoza, with the name of "GTCLC-NEG". The project aims at promoting a Carbon Negative Technology, capable to burn multiple biofuels derived from biomass (eg, pyrolysis oil, biogas and syngas) and to capture the CO_2 emissions at a very low cost. In this way there will be negative GHG emissions, due to the use of BECCS (Bioenergy with Carbon Capture and Storage), a technology which needs to be developed and implemented within 2050, according to the IPCC. The proposed plant is based on the coupling of a Chemical Looping Combustor to a turbo expander, as proposed in Fig. 1.

As can be seen from Fig. 1, in the proposed plant compressed air is used to oxidise the oxygen carrier in the air reactor, and then it is expanded in a turbo expander to produce electricity. In the fuel reactor biofuels (eg. biogas, biomethane, syngas, pyrolysis oils, biodiesel, bioethanol and pulverised solids biofuels) are used to reduce the oxygen carrier. The gases exiting the fuel reactor are mainly composed by CO_2 and water vapor. They can also expand in a turbo expander and provide further electrical energy, although it should be considered that the flow in the fuel reactor is considerably lower than that in the air reactor. Further, the fuel reactor gas stream could contain impurities from the fuel conversion process, which should be minimal in the air reactor where no fuel conversion takes place. After the expansion process the gases can exchange their residual energy with a Heat Recovery Steam Generator (HRSG) and then the water vapor contained in the gases exiting the fuel reactor can be condensed and separated from the CO_2, which is sent to a compression section that at the end will produce liquefied CO_2. In the same way also the gases which have expanded in the turbine at the exit of the air reactor are used to recover heat to produce steam. So, two different HRSGs are needed, because we cannot mix the two flows of gases exiting the air and the fuel reactor. The vapor produced by the two HRSGs can be sent to a steam turbine (in this case we have assumed to use 2 steam turbines, because we want to have an idea of the energy which can be produced separately at the AR reactor and at the FR reactor).

1.2. Scope and novelty of the work

In this work starting from the literature data on pressurised chemical looping reactors we try to propose a new way to design PCLC power plants, based on the mass flow of the prime movers (gas expanders and steam turbines), which are coupled to the combustors. The idea is to present a viable process for achieving negative emissions. The data provided will be useful not only to people working in the sector of fluidised bed combustors and chemical looping, but also to experts in the fields of bioenergy, thermal machines and power plants.

The main advantage with chemical-looping has been established previously, and is based on the fact that no separation equipment is needed to obtain CO2 in pure form. Still, most previous works have been devoted mainly to fossil fuel conversion at atmospheric conditions. Here we want to propose a design based on a pressurised system, which could be applicable for the use of biomass-based fuels. Conventional design of chemical looping plants has been very clearly described in the publication of Kronberger et al. 2005 [11]. In this work a first set of design specifications, is put at the top of the methodology flowsheet. As an example of these specification we can consider: the thermal power of the CLC plant, the operating pressure, the fuel type and the oxygen carrier type. Then there is a second set of design specifications which are placed

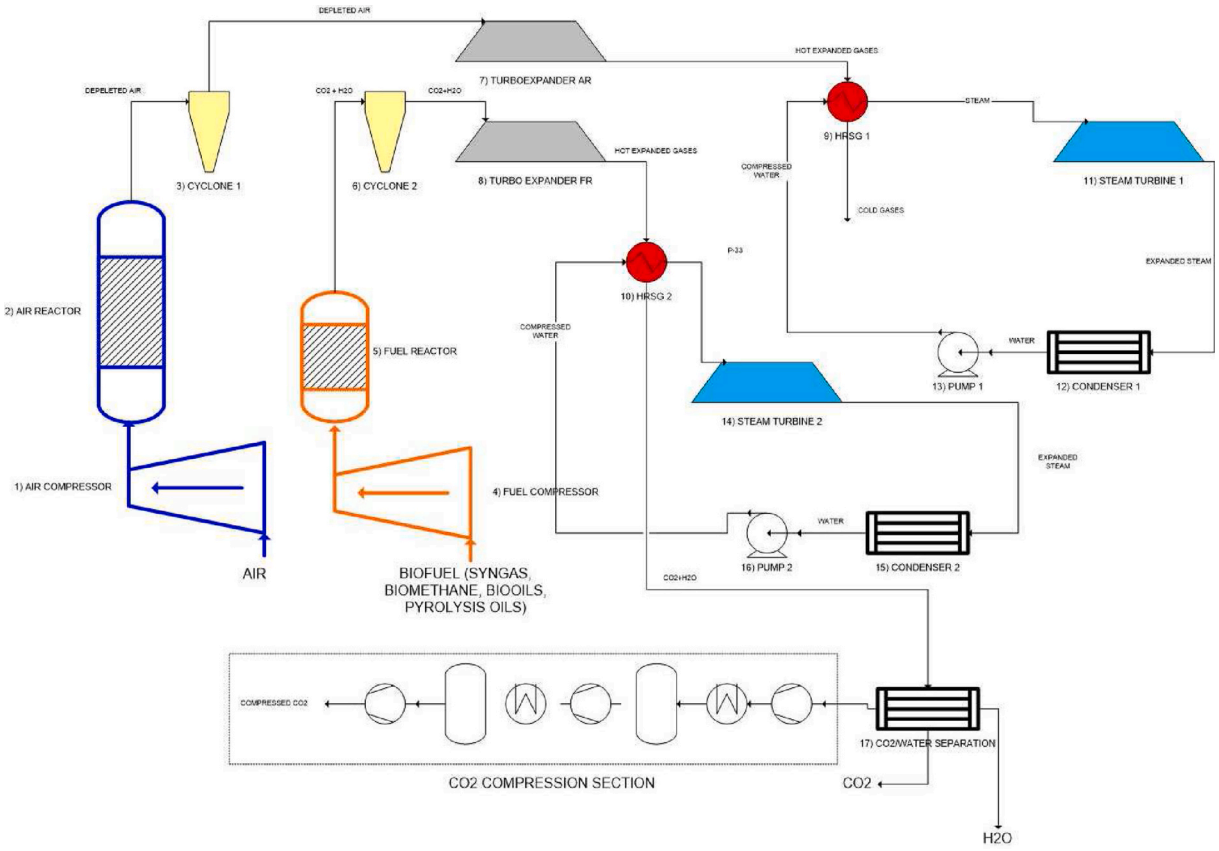

Fig. 1. The GTCLC-NEG concept.

at the bottom of the methodology. These are: reactor geometry, bed pressure drop, the solids circulation system. In the middle between the two design specifications we find: reaction kinetics (temperature, carrier reactivity, gas conversion, carrier capacity, solids conversion); bed hydrodynamics (bed operating regime, solids entrainment rates, gas leakage, residence time distribution, system pressure loop); design criteria (fuel mass flow, air/fuel ratio, solids circulation rate, bed mass).

If in the case of conventional CLC plants, the objective is trying to optimize their fuel conversion rate and CO_2 selectivity, in the case of PCLC coupled to turbo expanders the objective is to maximize plant electrical efficiency. In this case we start from the power capacity of the turbo expander, its optimal turbine inlet temperature and compression ratio and we define the characteristics of the air reactor and then we design the fuel reactor main specification and we calculate oxygen carrier inventory and circulation rate. Finally we have to propose a strategy to optimize plant electrical efficiency. The need to use PCLC is due to the highest efficiencies which can be achieved in a combined cycle respect to a steam cycle. While steam cycles using chemical looping combustion have been already realised on a pilot scale, combined cycles which need to use PCLC combustrs coupled with turbo expanders have not been yet tested on the pilot scale.

With respect to these aspects, this work can be considered new and has also a relevant impact for both sectors of power generation and chemical looping combustion. The authors believe that pressurised chemical looping combustion is a key technology to increase process efficiency and to perform process intensification and achieve advantages which are both economic and technical. Still the technology needs to be fully developed, especially with respect to pressurization, where there is very little previous work done.

1.3. Technical barriers regarding the coupling of a pressurised chemical looping combustor with a turbo expander

Possible technical barriers for the development of a pressurised chemical looping combustor, coupled with a turbo expander are:

(1) high efficiency oxygen carriers are needed, with high melting temperature, given that a high Temperature at the Inlet of the Turbine is needed to maximize plant efficiency (working temperature of 1200 °C will be probably needed);
(2) low attrition rates of the oxygen carriers are needed, allowing them to work in extreme conditions;
(3) kinetics aspects under high pressure and temperature conditions are still not completely known;
(4) reactor injection system has to be adapted to biofuels;
(5) the use of the hot air produced from the air reactor (see Fig. 1) in a turbo expander has to be optimised;
(6) exhaust gases should be properly treated to retain the dust released by oxygen carrier attrition;
(7) high electrical efficiency of the power system has to be granted, together with high fuel conversion in the combustor [12–14].

While the electrical efficiency of the turbine surely depends on the inlet temperature of the gases exiting the air reactor and the pressure at which they are fed into the turbine, we have to consider also that from an overall perspective the total thermal efficiency of the plant depends on the degree at which heat integration is performed. Based on the layout reported in Fig. 1 we can identify two main sources of waste heat:

- the exhaust gases which exit the turbo expander;
- the gases exiting the fuel reactor.

Dealing with the temperature at the outlet of the turbo expander, in principle this should not differ too much from that already measured for externally fired gas turbines (EFGTs). If we take for example the publication of Barsali et al. 2015 [15], we can see that externally fired gas turbines have an outlet temperature of the expanded gases which is about 544 °C. On the other hand the temperature at the outlet of the fuel reactor can be comprised between 900 °C and 950 °C, see for example [16]. To study the two heat sources is of key importance to understand where to place, for example, a steam turbine to recover all the waste heat and perform a combined cycle, which could have an efficiency comparable to a natural gas combined cycle (NGCC) [17]. Dealing with the turbine inlet temperature, which coincides with the air reactor outlet temperature, this can range from 900 °C (in the case of microturbines) to 1200 °C (in the case of conventional gas turbines). The most convenient way to achieve these values is to regulate the outlet temperature from the air reactor with the excess air since the oxidation reaction enthalpies are generally sufficient to release the heat required to reach the targeted temperatures so no top firing is needed in most cases.

2. Pressurised chemical looping for power generation: main plants layouts, plants efficiency and reactors configuration

2.1. Pressurised Chemical Looping: power plants layouts

A classical layout for realizing a power plant with PCLC is that reported by Ishida et al. 2002 [18,19].

This is an interesting layout that we can summarize as a PCLC reactor where the air reactor provides a fluid to be expanded in a turbo expander and the fuel reactor provides a hot flow of carbon dioxide and water vapor, which is used in a Heat Recovery Steam Generator (HRSG) to recover part of its enthalpy to produce vapor to be expanded in a steam turbine. The steam turbine will expand also the vapor produced from the exhaust gases which previously expanded in the turbo expander. This is a promising configuration, because it can use all the enthalpy of the gases exiting the fuel reactor and it is less expensive than other solutions, in which the gases exiting the fuel reactor are expanded in a turbo expander and then the waste heat is further recovered in a HRSG. A solution using two expansion turbines is provided in Ref. [20].

A similar approach to the one of Ishida [18] is proposed also by Wolf et al. 2005 [21]. While the plant proposed by Ishida works at 20 bar of pressure, the plant studied by Wolf and Yan mainly worked at pressures comprised between 9 and 13 bar.

The concept of plant provided by Wolf et al. 2005 [21] was further refined in the CLC extended combustor, as we can see from Fig. 5.

In the extended CLC combustor, developed by Wolf and Yan 2005 [22], the combustor consists of an air reactor and a fuel reactor where the fuel is oxidised in sub stoichiometric conditions also adding steam, to perform reforming and produce a syngas rich in hydrogen. In the same fuel reactor, which is used as a reformer; also calcium oxide is introduced to absorb CO_2 and increase H_2 concentration in the produced syngas. The calcium carbonate ($CaCO_3$) formed in the reformer is then transferred to a calcination reactor, where it is converted again to calcium oxide, to begin the cycle again [22].

Another reactor configuration it is considered in the CLC3 option (see Fig. 6), which has been described in the work of Chiesa et al. 2008 [17]. The pressure of the CLC reactor in this case is about 20 bar.

This configuration needs to use an oxygen carrier with multiple oxidation states, so for this reason iron is considered to be the preferred oxygen carrier. The CLC3 plant is based on two oxidation reactors (where air and steam oxidations are performed) and one reduction reactor. FeO is oxidised in the steam reactor to produce Fe_3O_4 and hydrogen. Fe_3O_4 is then completely oxidised in the air reactor to Fe_2O_3. Then in the fuel reactor Fe_2O_3 is reduced back to FeO. As it was in the previous case, also in this case the outputs of the reactor are: depleted air, pure CO_2 and water vapor.

As it can be seen from the plants layouts presented in Figs. 2–6 in most of the cases we have plants where combined cycles are performed and in some cases the plant is used also to produce fuels. A different case, in which we have instead only a turbo expander is represented by the plant developed at the MIT and described in Ref. [23] (see Fig. 7). In this

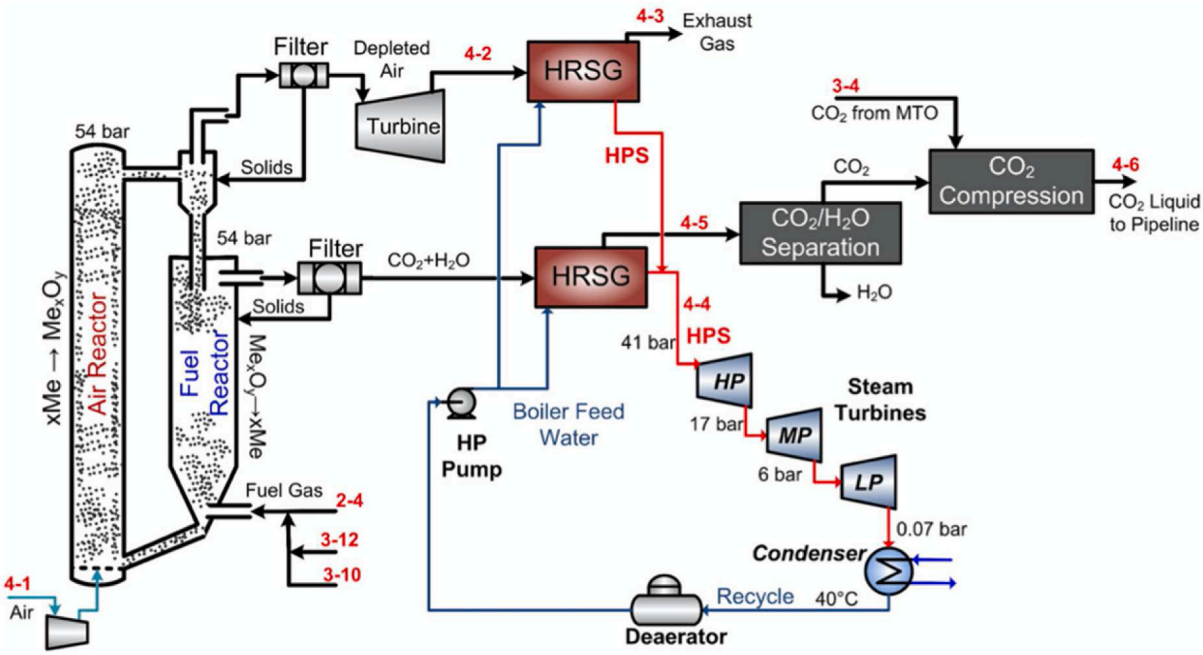

Fig. 2. PCLC combined cycle according to Ishida et al. 2002 [18,19].

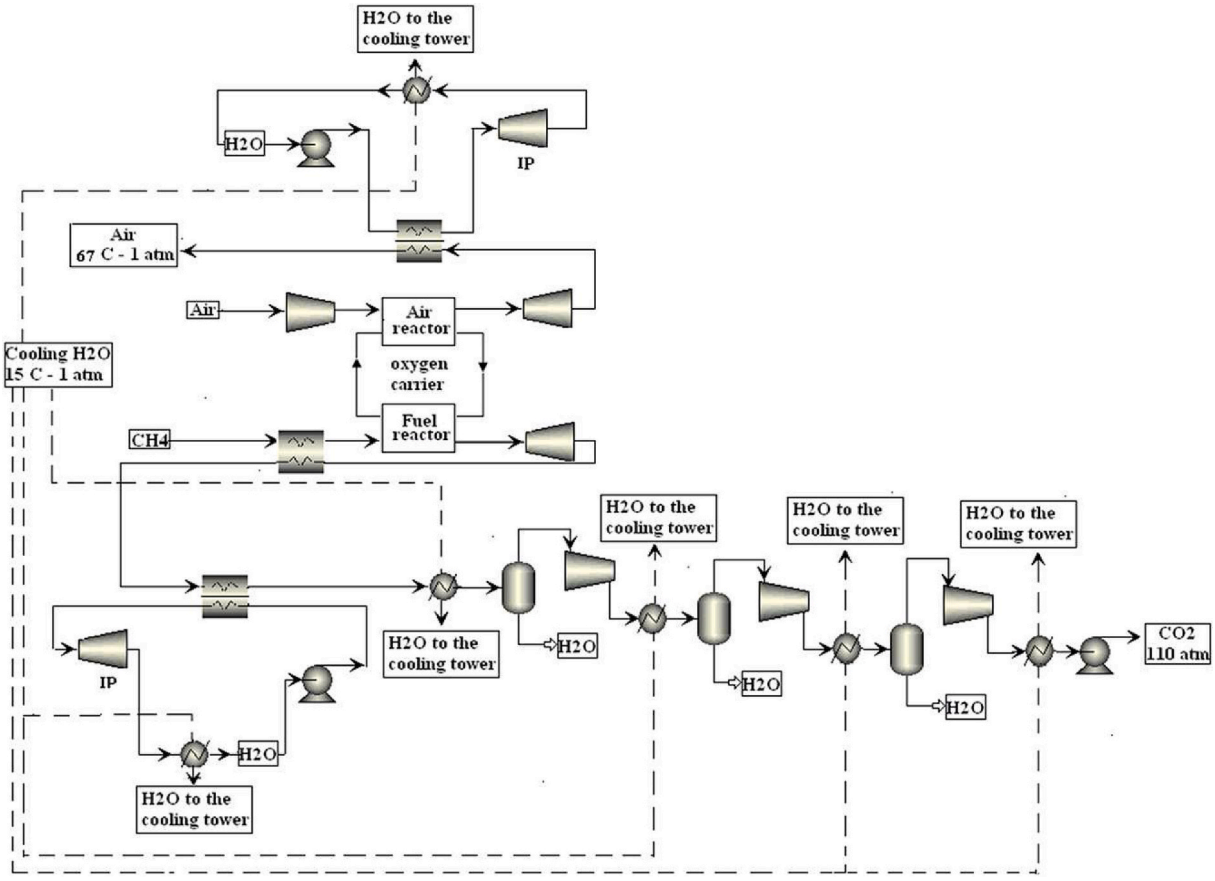

Fig. 3. PCLC power plant according to Porrazzo et al. 2016 [20].

case the compressor pressure ratio was set to about 5.

The waste heat coming from the turbo expander is used to regenerate the turbine itself, so there is no need to introduce a combined cycle.

The issue of heat integration among different layouts has been taken into account, for example, in the publication of Petriz-Prieto et al. 2016 [24]. This is an interesting study which compares different reactors configurations: the conventional CLC combustor (see Fig. 2); the extended CLC combustor (see Fig. 5); the CLC3 option (see Fig. 6).

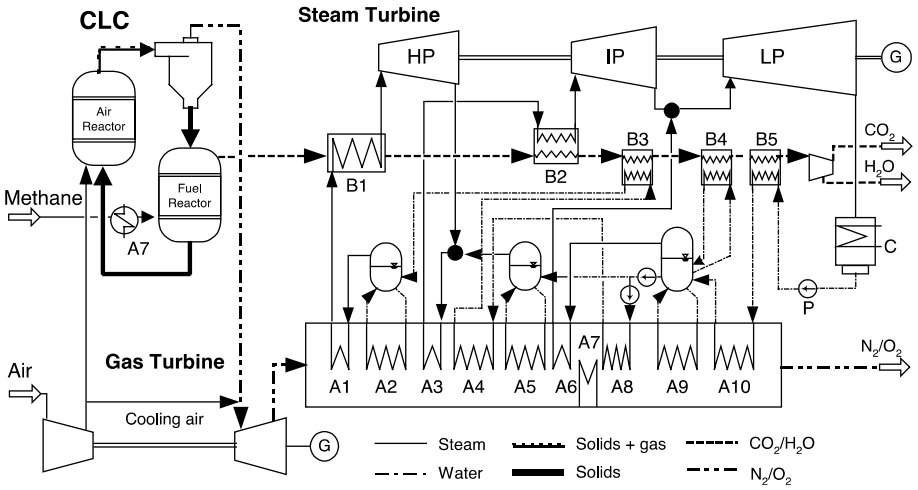

Fig. 4. PCLC power plant according to Wolf et al. 2005 [21].

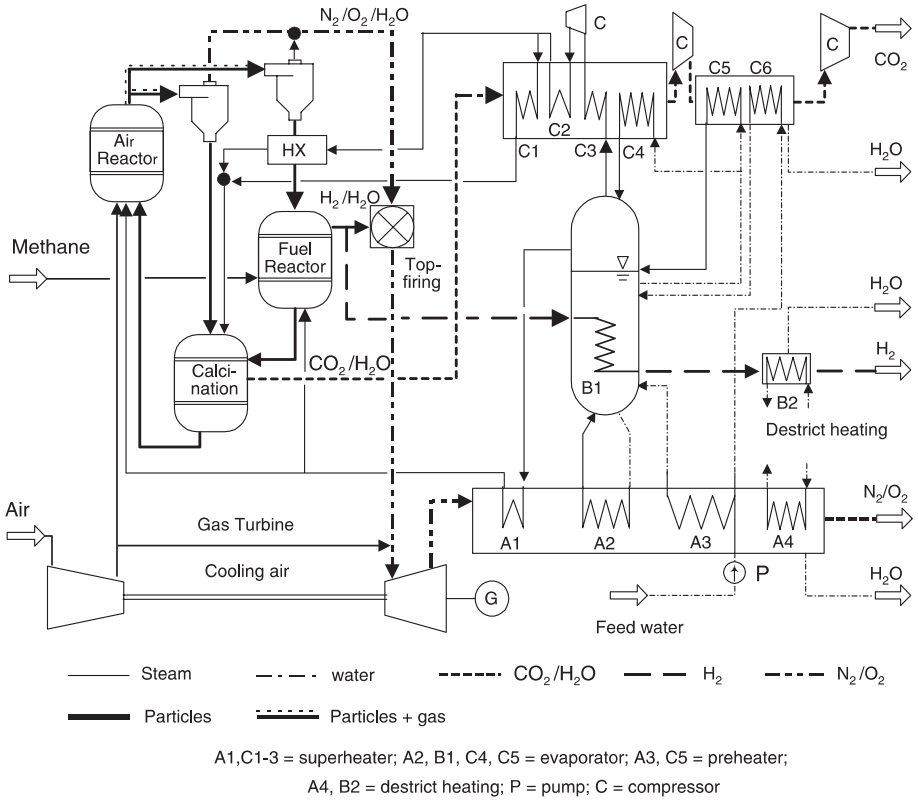

Fig. 5. The exCLC-STIG process [22].

These three plants configurations can be coupled to three other power generation technologies (see Ref. [24]), such as: a combined cycle steam injected gas turbine (STIG cycle), a Humid Air Turbine cycle (HAT) or a simple steam cycle. In Ref. [24] it is scarcely discussed the possibility to insert a burner to increase the temperature at the exit of the air reactor (i.e. top firing). This possibility is instead reported in Ref. [25]. Top firing can be importantly beneficial to the final plant efficiency; it can be performed with natural gas, as reported in Ref. [25]; but it can also use hydrogen [26] (in this way avoiding emitting CO_2 during the combustion process). In theory also a oxyfuel post-combustor could be installed after the air reactor and before the turbine to increase the temperature of the gases without causing any penalty in CO_2 capture (which will be on the other side caused by the use of natural gas as a fuel for the post combustor, when air is used as oxidizing agent).

An interesting contribution on the potential integration of chemical looping combustion into power generation is provided by the work of Zerobin and Pröll 2017 [25], which has been developed in the framework of the SUCCESS project, funded by the European Union under the 7th Framework Programme. The plant proposed in Ref. [25] is shown in Fig. 8. In this case the reactor working pressure varied between 4.96 bar and 6.72 bar.

A more updated study, published through the collaboration of Department of Energy at Milano Polytechnical University (Italy), SINTEF Industry (Norway), NTNU (Norway) and VITO (Belgium) [26] has shown higher efficiencies, in particular it has demonstrated that with certain configurations the CLC-CC plant can achieve almost the same

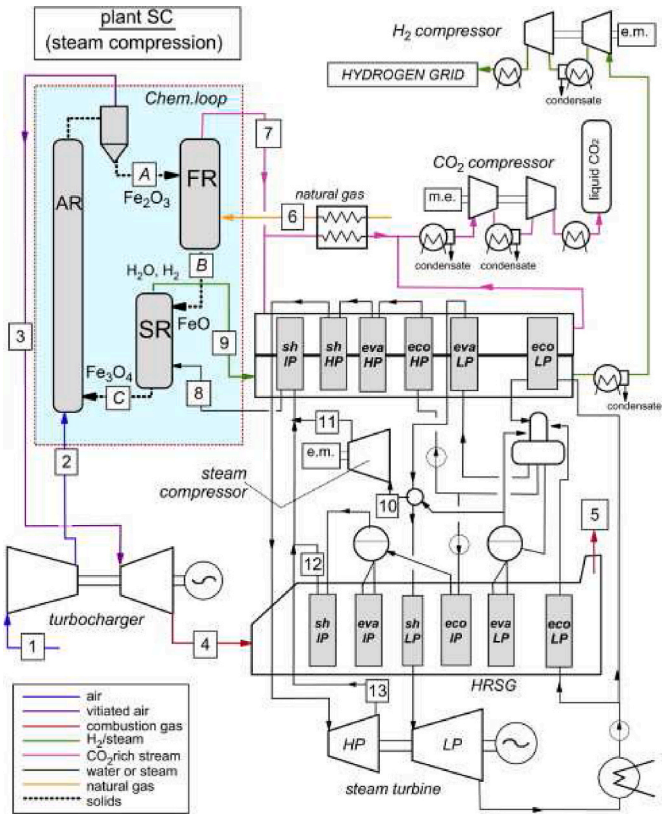

Fig. 6. The CLC3 plant developed by Chiesa et al. 2008 [17].

total efficiency of a NGCC (loosing only 1% point). The plant proposed in Ref. [26] is shown in Fig. 9. In this case the compressor pressure ratio is about 23.6.

We see that the plant uses an Internally Circulating Reactor (ICR) and a combustor, which is fired with H_2 and also fed with steam to increase the volume of gases expanding into the turbo expander. This can imply also the increase in power production. So in this way it is not necessary to use a turbine at the exit of the fuel reactor to produce the required electricity to compress the CO_2 again. A two-phase heat exchanger is used to preheat the H_2 and the water (which is evaporated and forms steam) to be fed to the combustor. The heat is given by the CO_2 and water exiting the fuel reactor, which are cooled down to condense the water.

All the plants shown above are mainly fed with gaseous fuels (hydrogen in the case of [19] and natural gas in all the remaining cases). This means that if biofuels have to be used the most close case would be using biomethane, biogas or syngas For the use of solid or liquid biofuels further research and development would be needed.

2.2. Pressurised Chemical Looping: power plants efficiencies

If we refer to the plant in Fig. 8, this is based on the following turbo expander: Siemens SGT5-4000F with a nominal electric output of 307 MW and a turbo expander single-cycle efficiency of 40.0%, according to Ref. [25].

Given that both the air reactor and the fuel reactor produce hot exhaust gases, which also have a quite similar final temperature (about 900 °C in case of not using the after burner), it is assumed to connect the outlets of the two reactors (air and fuel) to two turbo expanders. In this respect, we have to consider that the mass flow of the exhaust gases from the air reactor is importantly higher than that of the fuel reactor. It has also to be considered, for example, that the temperature inside the air reactor is regulated by venting excess combustion air inside it [27]. For this reason, the electrical capacity of the turbine connected to the exit of the air reactor will be much higher than the capacity of the turbo expander connected at the outlet of the fuel reactor. The CO_2 expansion in the turbine connected to the fuel reactor will provide basically part of the electricity requirements to recompress it for final storage (once it has been separated from the condensed water). In this way the combined cycle HRSG results to be more complex than that needed for a simple NGCC because the exhaust gases flows are two in the case of a Chemical Looping Combustor, while we have only one flow in the case of a natural gas combined cycle. Interestingly the CLC-CC plant shown in Ref. [25] extracts part of the low pressure steam from the turbine to satisfy the requirements needed to produce gas to be used in the loop seals. The main technical barrier to be addressed in the proposed process is represented by the need to remove the small oxygen carrier particles (generated for example by the attrition inside the bed and the

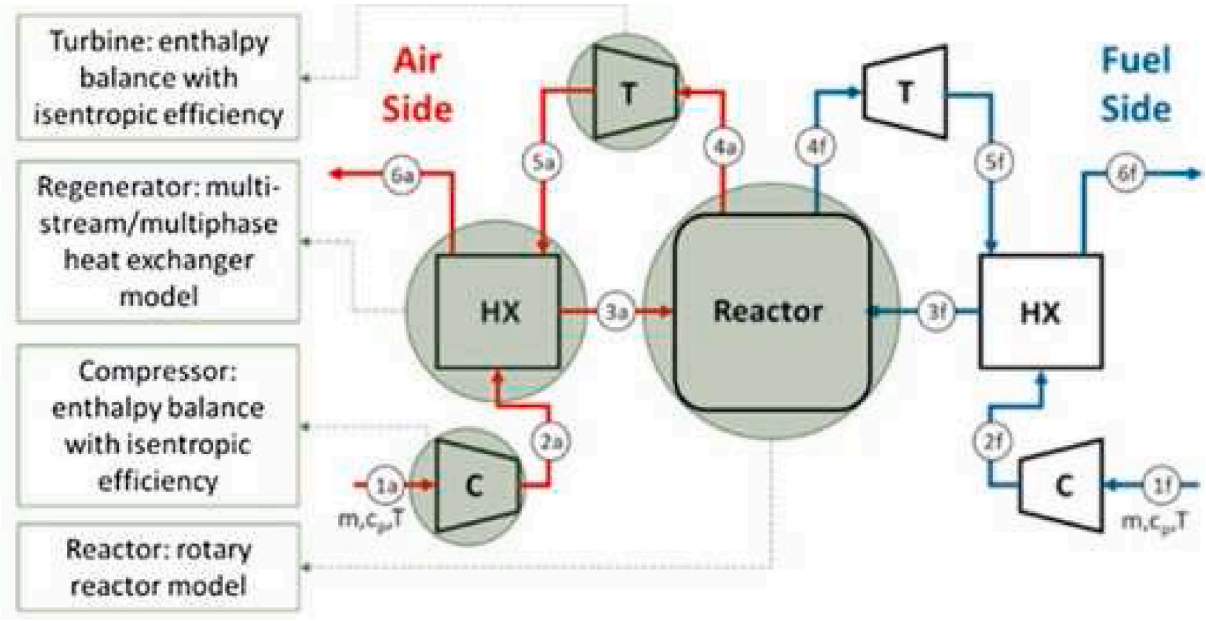

Fig. 7. Rotary chemical looping (recuperative Brayton cycle) [23].

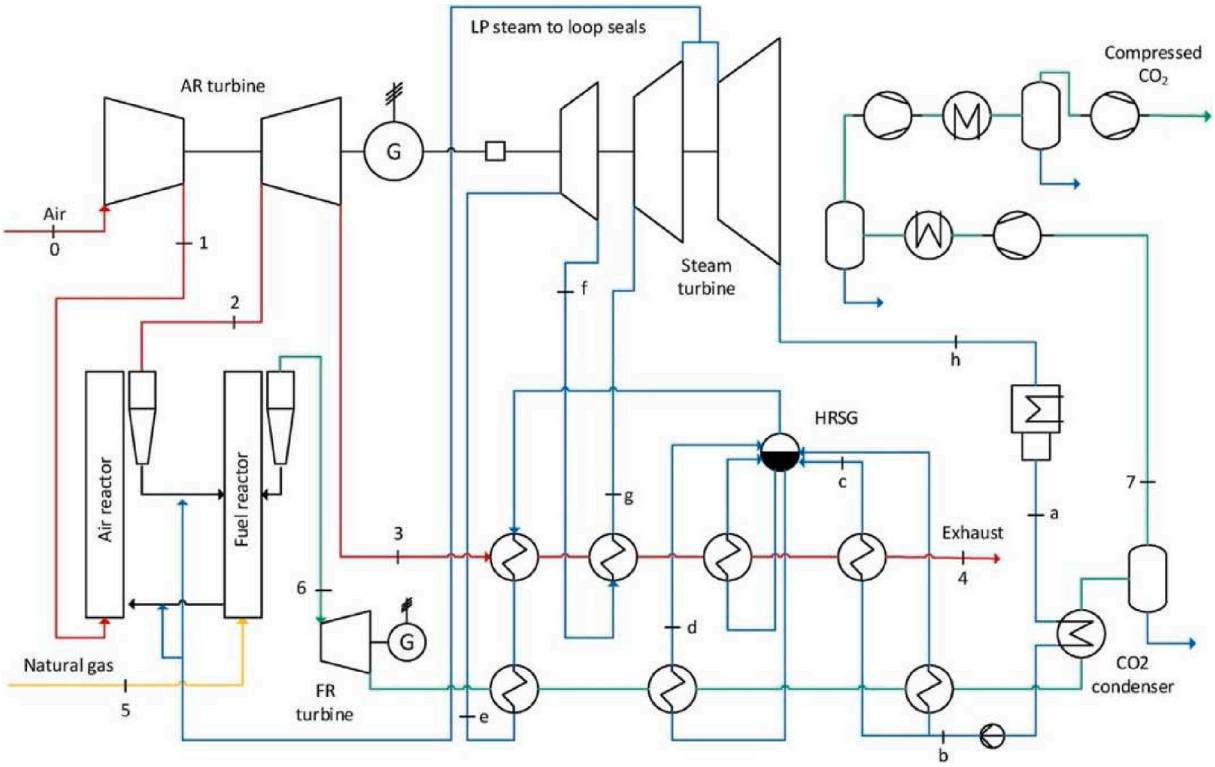

Fig. 8. CLC combine cycle process with CO_2 compression [25].

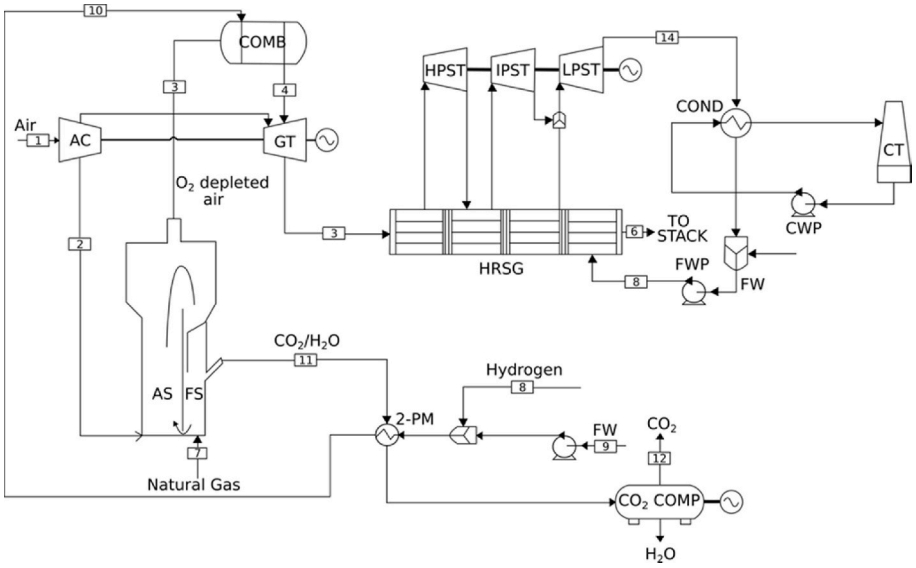

Fig. 9. ICR-CC plant with topping-combustion using hydrogen and a two phase flow heat exchanger. Adapted from Ref. [26], where AC is the air compressor, AS is the Air Section, FS is the Fuel Section, COMB is the combustor, GT is the turbo expander, 2-PH is the Two Phase preheater, HRSG is the heat recovery steam generator, HP/IP/LP is the High/Intermediate/Low pressure, ST is the Steam Turbine, COND is the condenser, CT is the cooling tower, CWP. Is the cooling water pump, FW is the feed water, FWP is the feed water pump.

consequent elutriation and lack of efficient removal by the cyclone).

In the analysis of [25] two scenarios are taken into account: without top-firing and with top-firing. In both cases the pressure used in the fuel and in the air reactor is about 5 bar, which is quite low, but it is demonstrated that the efficiency of the plant is more deeply influenced by the Turbine Inlet Temperature, as will be explained later. Before taking into consideration the final electrical efficiency of the plant, we can consider that Naqvi et al. [28] obtained a full load efficiency of about 52.2% and Porrazzo et al. [20] obtained a value of 52.4% with the air reactor working at 1200 °C and the compression of CO_2 at 110 bars (comprised). Finally the study of [25] arrives at the conclusion that despite the interesting values shown in Table 1 and the efficiencies reported by other scientists a more realistic estimate of the final electrical efficiency of the plant should be based on the following assumptions:

- temperature of the fuel and air reactor, set to a maximum of 900 °C
- pressure drop in the entire CLC reactor system of 1000 mbar;
- fluidization steam mass flow of 50 t/h;
- 100% capture of CO_2;
- CO_2 compression at 110 bar.

With these assumptions a net electrical efficiency of the CLC-CC plant of about 42.10% can be derived. The authors suggest also that

Table 1
Electrical efficiency of CLC plants integrated in power generation.

Source	Electrical efficiency (%)
[24], Simple CLC, Ni, Steam Cycle	50.25[a]
[24], Simple CLC, Ni, STIG	50.49[a]
[24], Simple CLC, Ni, HAT	56.08[a]
[24], Simple CLC, Fe, Steam Cycle	49.92[a]
[24], Simple CLC, Fe, STIG	50.28[a]
[24], Simple CLC, Fe, HAT	56.60[a]
[24], exCLC, Ni, Steam Cycle	52.58[a]
[24], exCLC, Ni, STIG	49.96[a]
[24], exCLC, Ni, HAT	52.34[a]
[24], exCLC, Fe, Steam Cycle	49.99[a]
[24], exCLC, Fe, STIG	45.81[a]
[24], exCLC, Fe, HAT	47.73[a]
[24], CLC3, Ni, Steam Cycle	51.18[a]
[24], CLC3, Ni, STIG	49.76[a]
[24], CLC3, Ni, HAT	55.03[a]
[28], CLC-CC	52.2
[20], CLC-NGCC	52.04
[25], CLC-CC	42.10
[26], ICR-CC	39.3
[26], ICR-NG	59.3
[26], ICR-H2	59.3
[26], ICR-H2-2P	60.9

[a] The star indicates that the efficiency does not consider electricity requirements to compress CO_2, so it is gross electrical efficiency.

more energy penalties could occur in real cases, such as: non effective gas cleaning and pressure drops due to the use of heat exchangers. It is concluded from the analysis shown in Ref. [25] that the greatest energy penalty of the CLC-CC plant is due to the reduced turbine inlet temperature. Further energy penalties are represented by the requirements of steam for sealing the gases in the air and the fuel reactor and to contrast the pressure drop which is due to the bed in the reactor. All these penalties imply that a realistic efficiency for a CLC-CC plant would be about 42.1%, while a NGCC plant with carbon capture and compression at 110 bar would have an efficiency of about 49.4%.

If the data presented in Ref. [25] are quite pessimistic about the use of CLC in power cycles, it has to be considered that the results of similar studies available in the literature are not always in agreement. More specifically CLC could find a niche market in the power production with carbon negative technologies, which is the topic of the GTCLC-NEG project. If much focus was put in this section of plant efficiency we must remember that one of the most important criticalities is linked with the operation in pressurised condition of the CLC reactor. If we assume to use a two coupled CFB reactors combustor configuration, we will have important difficulties in the operation of the loop seal in pressurised conditions, together with this problem other barriers which need to be addressed are: difficulties of circulation of the solids between the air reactor and the fuel reactor; large solids circulation rates imply pressure fluctuations in the reactors, that have to be controlled adequately using backpressure controllers; increase of solids entrainment can lead to clogging of the cyclones and damages of the turbo expanders. New prototypes of reactors are in development to overcome these barriers, as it will be introduced in the next sessions.

2.3. Pressurised Chemical Looping: reactor configuration

A first approach to the optimization of plant configuration is that based on the optimization of the single plant components, which in the case of the PCLC plant are the following [29]:

- heat exchangers (if any),
- solid separators,
- fuel and air injectors.

The research on PCLC reactors is still ongoing and there is not agreement on what could be the most optimal configuration. The key issue to address in PCLC reactors design and optimization is the circulation rate. This is deeply connected also with the functionality of the loop seals under pressure. For this reason a way to address the circulation problems when the reactor is operated under pressure is to check the working conditions of the loop seal, as performed in the work of Cheng and Basu [30]. They have noted that in the loop seal the solid recycle rate was increasing with the increase of pressure. This could be explained by two main phenomena:

1. the increase of the fluidizing gas density which happens with the increase of pressure makes it easier to support the weight of the particles even at a low velocity;
2. generally it has been noted that the minimum fluidizing velocity decreases with the increase of pressure.

In their work Cheng and Basu [30] noted also that the solids friction factor (f_{rs}), for the recycle pipe of the loop was measured to be around 2.9.

The problem of solids circulation is identified as one of the main challenges in the development of future CLC plants also by the work of Osman [31]. In this work it is highlighted that the circulation between the air reactor and the fuel reactor can present challenges, due to the need of accurate particle separation and of careful optimization of the loop seal. Some practical technical barriers to overcome on conventional CLC plants based on two CFB reactors are the following (especially when the plant is operated at high pressure):

- difficulties of circulation of the solids between the air reactor and the fuel reactor;
- large solids circulation rates imply pressure fluctuations in the reactors, that have to be controlled adequately using backpressure controllers;
- increase of solids entrainment can lead to clogging of the cyclones and damages of the turbo expanders.

The two most important case studies on new CLC reactors are represented by:

- the PFIR reactor developed by Canmet Energy together with Hatch Associates, which layout is illustrated in Fig. 10;
- the ICR reactor developed at Norwegian University of Science and Technology (NTNU).

The PFIR concept is based on the work of Adham et al. [32,33] which developed a reactor with multiple internal stages and non-mechanical control of gas solid flows to basically reduce the investment costs of the total plant, also referring to DOE recommendations on CCUS [34]. The plant concept is referred to as the “Plug Flow Internally-circulating Reactor (PFIR)” and consists of two reactive zones separated by baffles (see Fig. 10).

In particular, at NTNU Osman proposes the development of an Internally Circulating Reactor, which is completely similar to that already presented in Fig. 9. This has the advantage of substituting the cyclones and the loop seals which are mainly involved in solids circulation with ports which are installed in two sections of a single reactor (see Fig. 11).

The ICR unit shown in Fig. 11 is still a laboratory scale unit (thermal power of 5 kW) while the PFIR reactor is designed for the capacity of 600 kWth. The ICR unit has been operated from 1 to 6 bar, up to now. The optimal pressure is also reported to be about 4–7 bar for the PFIR reactor developed at CANMET.

Based on what has been above said here we propose a summary of the pros and cons of the described innovative concepts of reactors and their comparison with the so-called dual fluidised bed reactor or the interconnected circulating fluidised beds. The last solution is the one

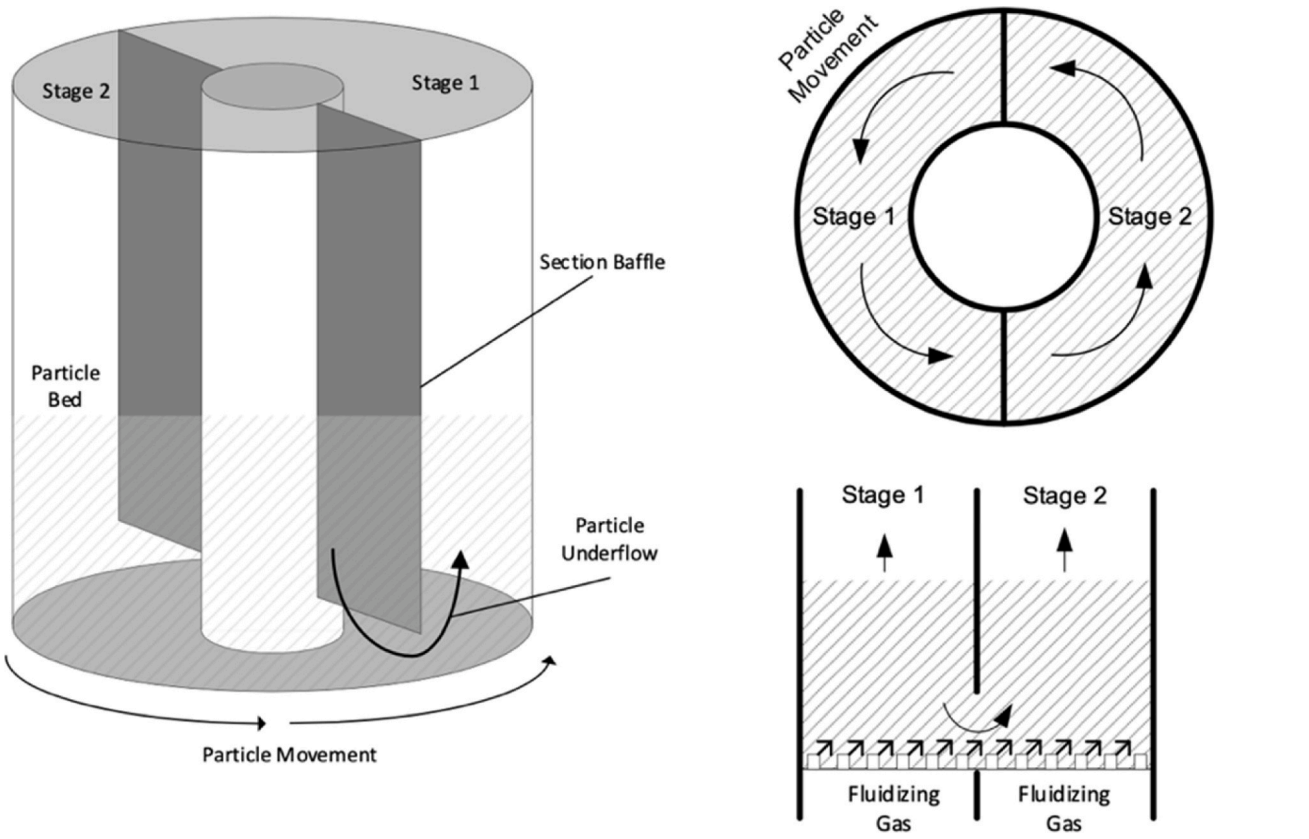

Fig. 10. Schematic of PFIR geometry. A) 3-dimensional view B) Top-down view C) Side view of stage transition [35].

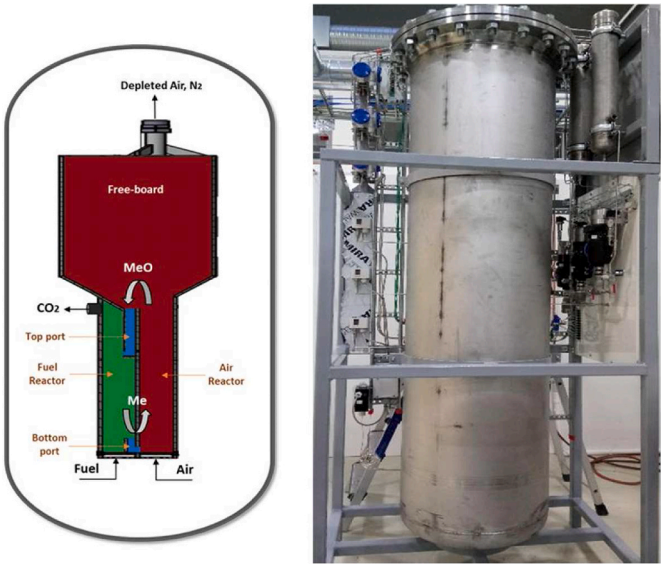

Fig. 11. Simplified scheme of the ICR design (left), and the ICR unit under operation inside the shell (right) [31].

which has been proven at higher thermal power scales of the combustor (see Table 2).

3. Effect of pressure on fluidised bed hydrodynamics

According to the book of Alvarez and Anthony on pressurised fluidised beds [36] the pressure has effects on the following phenomena:

Table 2
Pros and cons of different reactors configurations.

Reactor type	Pros	Cons
Dual fluidised bed reactor	Already available at higher scales High number of working hours Higher reliability Avoids gas leaked between the fuel and the air reactor	Higher investment cost Problems due to pressure management and pressure inbalance in the loop seals Need to optimize the circulation rate Need particle separation systems Pressure losses arise from the use of high temperature high pressure cyclones Unwanted pressure fluctuation due to imperfect back pressure-controllers Higher attrition problems
PFIR	Lower investment costs because uses a single reactor vessel Avoids use of loops seals Large flow rate of solids enabled Solid movement enabled by angled jets at the distributor Working in the bubbling regime Reduced mechanical parts movement No external solids circulation	Possible gas leakage between air and fuel reactor Circulation rate measurement challenges Possible low carbon dioxide purities Possible High Volume of the reactor required
ICR	Lower investment cost Avoids use of loopseals No external solids circulation Good fuel conversion efficiency	Possible gas leakage between air and fuel reactor Possible low carbon dioxide purities Tested only in lab

- minimum fluidization velocity;
- effect of bed voidage;
- effect on bubbling characteristics;
- effect on entrainment and elutriation;
- and dynamic scaling considerations.

These aspects are exactly those reported in Table 3 and we can add also that bubble dimensions and characteristics have an influence on heat exchange between the solid and the gaseous phase.

The details of the effect of pressure on: gas density and viscosity, solids-gas and solids-solids interactions, minimum fluidization velocity, bed expansion height and emulsion voidage, bubble characteristics, circulation rate, bed particles behavior depending on Geldart group are proposed in the supplementary material to this paper.

In the end it has to be considered that the increase of pressure will decrease the minimum velocity for fluidization, while leaving the same bed voidage.

Dealing with bubbles behavior, by increasing the bed pressure at an excess gas velocity (Ug- Umf) the following phenomena can be observed: increase in bed expansion [37–43], decrease in bubble size and bubble splitting, increase in bubble passage frequency [38–41,43–49], increase in visible bubble flow rate [38–41,43,47], increase in bubble rise velocity (Ub) [38–41,43–45,47], bubble phase fraction [38–41,43], solids concentration in the bubble phase [48,50] and the tendency of bubbles to pass through the central axis of the reactor [38,43,44,47]. While pressure enhances bubble splitting, it also enhances their coalescence, see Refs. [43,44].

Dealing with the emulsion phase, the emulsion phase voidage increases with pressure (see Refs. [43,48,50]), while the emulsion phase fraction will decrease. Bubbles coalescence is responsible for the higher flow of bubbles in correspondence to the vertical axis of the reactor [51] It is very interesting to note that the concentration of the bubble flow in correspondence to the vertical axis of the reactor promotes the circulation of solids inside the bed [44,51]. The concentration of bubbles in the vertical axis of the reactor can explain the increase of Ub, due to the increase of pressure even with a smaller diameter of the bubbles [43].

The above reported changes will result basically in an improvement in solids mixing for moderate and coarse particles. The better mixing is also explicable with an increase in the drag force. The increase in the solid gross circulation, together with the increase of the granular temperature [50], can lead to the decrease of the critical velocity (U_c), see Refs. [52–56]. This decrease of Uc is coupled with a decrease of also Ut, which is linked with an increase in solids entrainment [56–61]. This is a very interesting aspect of PCLC reactors. The increase of hydrodynamic forces in the bed, caused by the increase in pressure results also in an increase in jet penetration length (see Ref. [62]) and transport disengagement height (see Ref. [60]). On the other hand the choking velocity decreases (see Ref. [63]). The better mixing of the solids can result also in an increase of electrostatic forces (a form of interparticle forces). A summary of the effects of pressure on fluidised bed behavior is presented in Table 4.

The information shown in Table 4 can be used for the design of the reactor through the use of modeling software. For both: CFD models and 0D models it is important to know how the main governing equations are influenced by pressure. We see that the knowledge of the effect of pressure on kinetics, thermodynamics, fluidization and heat transfer phenomena is key to the design of efficient reactors.

Table 3
Effect of pressure on the hydrodynamics of a fluidised bed combustor, adapted from [10].

Hydrodynamic parameter	Effect of pressure
Minimum fluidization velocity u_{mf}	Increasing pressure decreases u_{mf}. This effect becomes more pronounced as the particle size increases.
Bed voidage	- There is no clear correlation between pressure increase and bed expansion. - ε_{mf} is independent of pressure. - ε_{mb} increases with pressure for particles close to the group A-B boundary.
Bubbling characteristics	High pressure results in smaller, more frequent bubbles. These effects are more pronounced for group A particles than for group B ones.
Entrainment and elutriation	- The bubble flow u-u_{mf} increases with pressure, leading to higher entrainment rate. - The terminal velocity decreases with increasing pressure (due to the increase in gas density), hence enhancing the entrainment/elutriation rate.
Hydrodynamic scaling	Unlike atmospheric fluidised-bed reactors, cold flow laboratory model (operating with air at ambient temperature and atmospheric pressure) of a pressurised fluidised-bed at 12 bar and 860 °C is approximately the same size as the commercial unit [36]

4. Biofuel combustion in Pressurised Chemical Looping reactors: kinetics aspects

4.1. BECCS based on chemical looping combustion

A complete review of the technologies developed using biofuels in Chemical Looping is provided by the paper of Mendiara et al. 2018 [7]. The main processes identified are the following:

- Chemical Looping Combustion (CLC);
- Chemical Looping with Oxygen Uncoupling (CLOU);
- Chemical Looping Reforming (CLR);
- Chemical Looping Gasification (CLG);
- Chemical Looping Coupled with Water Splitting (CLWS).

For the sake of this paper the interest is mainly focused on Chemical Looping Combustion, because we believe it is the process which can be better coupled to a turbo expander. Together with the classification of the possible Chemical Looping Processes, which can be used in BECCS also the types of biofuels which can be possibly used are proposed:

Table 4
Summary of the influences of increasing pressure on the hydrodynamics of gas-solid fluidised beds [64].

Hydrodynamic characteristic	Fine powders
ε_{mf}	–
U_{mf}	Depends on particle type
Homogeneous bed expansion	↑
ε_{mb}	↑
U_{mb}	↑
Bubbling bed expansion	↑
Bubble size	↓
Bubble passage frequency	↑
Visible bubble flowrate	↓
U_b	↑ or -
Bubble stability	↓
Bubble splitting & coalescence rates	↑
Solid concentration in the bubble phase	↑
Tendency of bubbles to pass through the bed close to the central axis	↑
Emulsion phase voidage	↑
Emulsion phase fraction	↑
Tendency of gas to interstitially pass through the bed in the bubbling regime	↑
Granular temperature	↑
U_c	↓
Solids entrainment	↑
TDH	↑
U_{ch}	↓
U_t	↓
Jet penetration length	↑

-: unchanged, ↓: decreasing, ↑: increasing.

- primary biofuels (which are mainly lignocellulosic materials and organic materials which have been not pre-processed by mechanical, chemical or biological treatments);
- secondary biofuels (which are lignocellulosic and organic materials which have been pretreated through mechanical, chemical and biochemical processes to produce biofuels of improved quality, such as: biodiesel, bioethanol, DME, biogas, syngas, etc.).

Biofuels are also categorised into: gaseous (eg. biogas, syngas, biomethane, pyrolysis non-condensable gases), liquid (eg. ethanol, biodiesel and pyrolysis oils) and solid biofuels (eg. wood chips and pellet). In Table 5 we present the main information from Ref. [7] on the use of gaseous and liquid fuels in continuous CLC units.

Dealing with gaseous fuels it has to be considered that gases have been already tested with satisfactory results at atmospheric pressure conditions, even though the problem of the siloxanes contained in biogas remains to be completely solved [70–72]. Same experience is available for syngas, biomass pyrolysis vapors and torrefaction vapors, which have all been tested at laboratory scale. Liquid fuels together with solid fuels have been tested also in continuous plants. The experience with liquid fuels is mainly based on the use of ethanol, as reported in Ref. [73]. In that case a continuous CLC plant of the thermal power of 1 kWth was used with bioethanol for 100 h. The oxygen carriers which were used were produced by impregnation on two main supports (γ-Al2O3 and α-Al2O3) and they were: Cu14–γAl, Fe20–γAl, Ni21–γAl and Ni18–αAl. In the last years experiments with solid fuels have been performed on a plant designed and realised at Chalmers university [67–69] also focusing on the effect of the release of alkali metals on the performance of the oxygen carrier. Among the cited studies very few are done at pressurised conditions.

4.2. Kinetic aspects linked with pressurised chemical looping combustion of biofuels

Both the reduction and oxidation reactions that happen in a CLC reactor are characterised by the kinetic triplet constants (activation energy, order of reaction and pre-exponential factor). The results we obtain in a Pressurised Thermogravimetric Analyzer (PTGA) can be influenced by the diameter of the oxygen carriers, their purity and their chemical characteristics and even the reaction conditions can have an influence. The kinetic triplets depend also on the model which is chosen, as we can see from one of the fundamental reviews on the subject (see Ref. [70]), that the models used to simulate the behavior of the oxygen carrier during the chemical looping process can be: Shrinking Core Model (SCM); Changing Gran Size Model (CGSM); nuclei growth model (NGM).

If we want to couple a CLC combustor with a turbo expander, we have to take into consideration that for the aim of the GTCLC-NEG process the kinetic triplets need to be derived at high pressure (with Pressurised TGA tests, see Table 6).

Pressurised Chemical Looping is well described in recent reviews [10], many works presented in Table 6 are taken from Ref. [10]. The new information available in this review is on the application of pressurised chemical looping combustion to the power sector and especially to turbo expanders. So it is important to show the final application of the kinetic constants to the practical design of PCLC plants coupled with turbo expanders in combined cycle power plants. Table 6 reports only reduction tests performed at high pressure, while CSIC and TU Eindhoven and also Canmet Energy have realised also oxidation tests at pressurised conditions [74,75].

According to Labiano et al. 2006 [76] the same kinetic triplets derived in pressurised conditions have some limitations, because together with pressure in the TGA also the effect of gas partial pressure, gas volumetric flow and sample mass have to be taken into account.

For what has been said above we will deal in the following paragraph on the effect of pressure on syngas and methane (or biomethane) that are the fuels which are more studied and tested up to now. To be complete, we have to take into account that the main advantage of PCLC will be in the future with solid fuels directly fed in the FR. It has also to be taken into account that there have been several commercial solid fuel PFBC combustors in operation and these ones are highly related to PCLC. A benefit of pressurised conversion of solids in the FR is also represented by the fact that the AR in this way results free from any corrosive compound, producing a quite clean stream of hot air which can evolve in the turbine without any arm by corrosive compounds (further attention has to be focused on the other hand on the arm which could be done to the turbine by the entrained powders of the oxygen carrier).

Table 5
Applications of biofuels in CLC units for BECCS.

Fuel Typology	Fuel	Scale	Source
Gaseous	Biogas	Laboratory scale	[7]
Gaseous	Syngas & Biomass Volatiles	Laboratory scale	[7,65,66]
Gaseous	Torrefaction vapors	Laboratory Scale	[7]
Liquids	Ethanol	Continuous Unit	[7]
Solid	Wood Pellets and Wood char, steam cured black pellets, Swedish wood char and German wood char	Continuous unit	[67–69]

Table 6
Pressurised TGA (PTGA) tests on oxygen carriers [77].

Group	Fuel	OC	Pressure Range	Source
CSIC, Spain	Syngas	CuO/Al_2O_3, Fe_2O_3/Al_2O_3, NiO/Al_2O_3	1–30 bar	[76,78]
USDOE	Syngas	NiO	1–7 bar	[79]
Southeast University	CO, Coal	Hematite	1–6 bar	[80–83]
The Ohio State University	CH_4, H_2	Fe_2TiO_5	1–25 bar	[84,85]
Eindhoven University of Technology	CO, H_2	CuO/Al_2O_3 $NiO/CaAl_2O_4$	1–20 bar	[86,87]
Canmet ENERGY & North China Electric Power University	CH_4, CO	$FeTiO_3$	1–24 bar	[88–90]
University of Kentucky	Coal char	$FeTiO_3$, Red mud	1–6 bar	[91]
University of Science and Technology Beijing	CH_4	Cu-based	1–9 bar	[92]
Korea Institute of Energy Research	CH_4	NiO, Mn_3O_4, CuO, Fe_2O_3	2–6 bar	[93]
University of Connecticut	CH_4	Ni & Cu Ocs	1–10 bar	[94]
Ningxia University	Coal	Fe_2O_3/Al_2O_3	1–10 bar	[95]

4.2.1. Biomethane

The results about the kinetic behavior of the oxygen carrier used to react with biomethane and syngas are derived from the PTGA tests presented in Table 6. PGTAs are quite complex instruments as can be seen in Fig. 12.

The HPTGA shown in Fig. 12 can reach a pressure of 30 bar and it is connected to several gas bottles to reproduce both oxidizing and reducing atmospheres. A similar device is available also at the Instituto de Carboquimica in Zaragoza Spain.

Among the studies presented in Table 6 there is already a good quantity of studies using methane as a reducing agent. Obviously, the results obtained with methane are fully comparable with those obtained with biomethane. So we can understand the behavior of biomethane in pressurised chemical looping by the following experimental experiences:

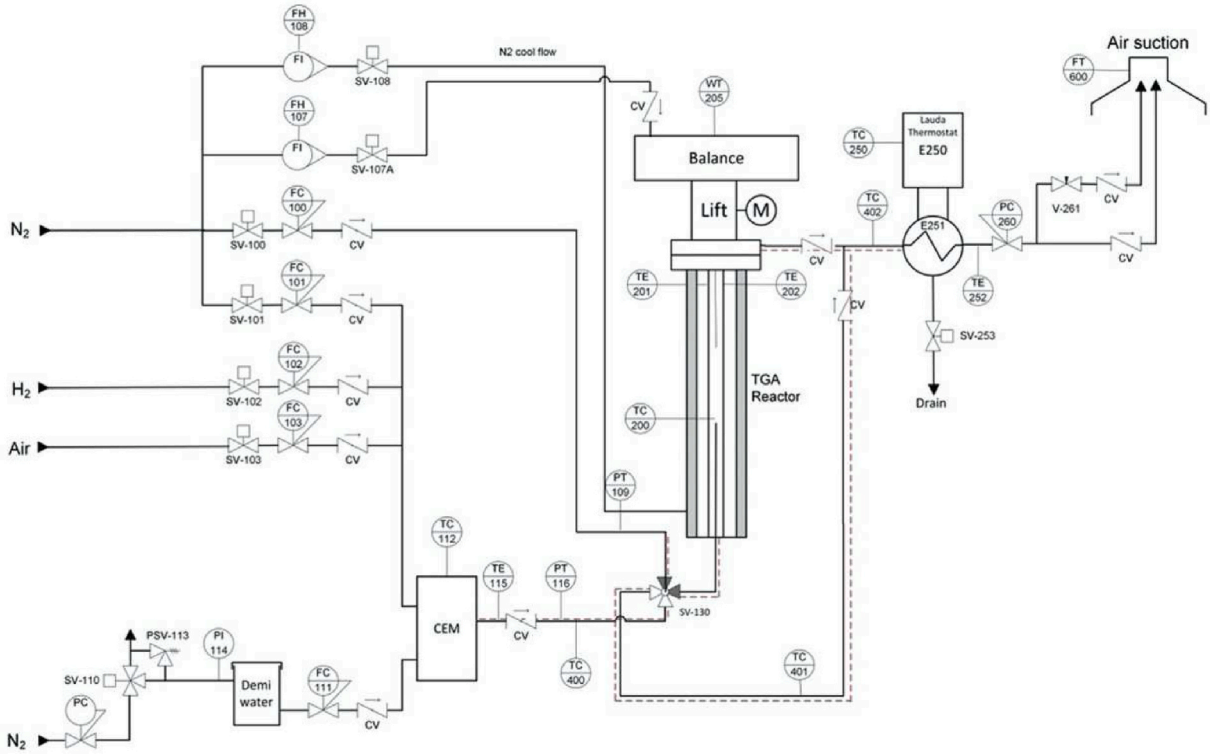

Fig. 12. Layout of the high pressure TGA (HPTGA) at the University of Eindhoven [87].

- an experimental campaign done with simulated natural gas by Canment ENERGY [89,90];
- an experimental campaign performed at the University of Science and Technology Beijing [92];
- one experimental campaign performed at the University of Connecticut [94];
- an experimental campaign performed in a reactor and described in the work published by the Korea Institute of Energy Research, the Korea Electric Power Corporation Research Institute and the Hanbat National University [93].

In the works of Canmet ENERGY the attention is focused on different parameters which can affect the kinetic behavior during the PTGA tests: the fuel partial pressure, the size of the particles and the weight of the oxygen carrier sample. According to the literature the tests have demonstrated that with the increase of pressure the reduction conversion rate decrease about 6–14% (for a pressure range of 0.9–1.6 MPa). The decrease in the reaction rate can be compensated by the increase of the fuel partial pressure.

The experiments discussed in Ref. [93] have been realised with a pressurised fluidised bed reactor, like the one shown in Fig. 13.

The reactor shown in Fig. 13 has a diameter of 0.025 m and a height of 0.312 m. The test procedure started with charging the oxygen carrier inside the reactor at atmospheric pressure and then beginning to heat the reactor up to 900 °C. Once the set point temperature was reached, the pressure inside the reactor was increased using the back pressure regulator. In the performed tests the pressure was varied between 3 and 6 bars and it was noted no particular change in the fuel conversion and in the CO_2 selectivity, which remained always very high.

An important information which is given in Ref. [93] is also a procedure to measure the attrition index of different potential oxygen carriers at pressurised conditions. Among those studied the one which performed best is the N016-R4, which showed and attrition index of only 5.4%.

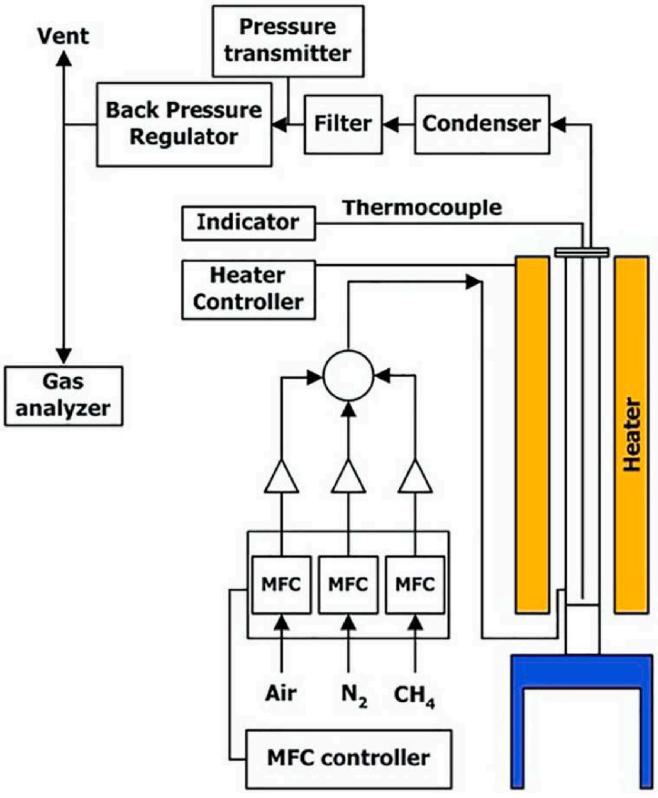

Fig. 13. Batch pressurised fluidised bed reactor [93].

4.2.2. Syngas

The main conclusions drawn from the tests performed on a PTGA at the Instituto de Carboquimica (ICB) in Zaragoza, with different oxygen

Table 7
Main insights obtained from PTGA tests using syngas as a fuel.

Parameter	PTGA behavior
Overall effect of pressure	- The effect of pressure causes a reduction in the reaction rate, compared to atmospheric conditions.
Solid conversion rate	- The solid conversion rate increases with temperature and syngas concentration. - The reduction rate of the oxygen carrier is not influenced by the concentration of reduction products (H_2O and CO_2). - The reactivity of the OC is influenced by the solid inventory used in the FR and needed to fully convert the syngas to H_2O and CO_2. - The solids inventory necessary to combust H_2 are generally lower than those required to combust CO in the fuel reactor.
H_2 reaction rate	- The reactivity of the OC with hydrogen is usually higher than that with the CO. - The reactivity of the OC in pressurised conditions depends strongly on the type of OC and cannot be modelled with kinetic parameters derived at atmospheric conditions.
CO reaction rate	- Solid conversion obtained with CO is much slower than that obtained with H_2. - The reaction order for the CO reaction (n = 1) is higher than that of the H_2 reaction (n = 0.8), this implies that the reaction rate for carbon monoxide becomes lower at high conversion of the syngas, and this implies that the trend of conversion of CO decreases and is less fast than that of H_2 (as already said).
Syngas reaction rate	- Syngas reaction rate behavior depends on the type of oxygen carrier; - In the case of iron based oxygen carrier the reaction rate of syngas is given by the sum of the reaction rate of H_2 and the reaction rate of CO.

carriers and different working pressures, see Refs. [78,96], are shown in Table 7.

The results of the experiments performed in Ref. [78] have shown interestingly that with Cu- and Fe- based oxygen carriers, the reaction rate of the oxygen carrier with syngas corresponded to the sum of the effects obtained using the individual fuel gases: CO and H_2. This is very important because it confirms that the approach of validating the model separately with H2 and CO is correct. Other important results of the experiments are:

- the reaction rate of hydrogen is generally higher than that of CO, so in chemical looping combustion in pressurised conditions hydrogen seems to be more reactive than carbon monoxide as a fuel;
- experimental analysis has shown that an increase in working pressure has a remarkable negative effect on the reaction rate of all the considered oxygen carriers and all the types of reactions (both reduction and oxidation);
- it was also noted that it is not possible to use the kinetic rate derived at atmospheric conditions to model what happens in pressurised conditions.

The solution to the discrepancy between kinetics at atmospheric conditions and kinetics at pressurised conditions was represented by an "apparent" pre-exponential factor described by Abad et al. 2007 [78] in the following way:

$$k_{0,p} = k_0 (P/P_0)^{pq} \quad (1)$$

Where k_0 is the pre-exponential factor at atmospheric pressure and $k_{0,p}$ is the pre-exponential factor at pressurised conditions, P_0 is atmospheric pressure and P is the actual pressure of the experiments, pq is the parameter calculated experimentally to relate the kinetics at atmospheric and pressurised conditions.

5. Effect of pressure on heat transfer

Dealing with heat transfer coefficients, these generally tend to increase with the increase of pressure, because of the influence of the convective heat transfer of the gaseous phase [97,98]. On the other hand Botterill and Desai [99] studied the heat transfer in pressurised fluidised beds and they found that elevated pressure has a better effect on improving heat transfer of large particles, while it has little effect on the heat transfer of small particles.

When heat transfer is influenced by pressure, an earlier transition from bubbling to turbulent bed behavior with the increase of the operating pressure has been noted.

The key mechanism used to model heat transfer in a fluidised bed is based on three main aspects [100,101], as reported in equation (2):

$$h = h_{pc} + h_{gc} + h_r \quad (2)$$

As it can be seen from equation (2), the components of the heat transfer equations are: particle convection (h_{pc}), interphase convection (h_{gc}) and radiation (h_r).

The above-mentioned quantities can be considered as independent one from another and their contribution is different, depending on different operating conditions. The radiative component becomes important only at temperatures which are above 873 K [97]. The particle component is highly dependent on the bubbling behavior, which generates the circulation of the particles inside the reactor. This component increases its importance for small particles diameters. With the increase of the dimensions of the particles the component of the gas convection increases its contribution. The gas convection contribution to the heat exchange increases also with the increase of the pressure, due to the increase in gas density.

The convective heat transfer can be expressed through the use of the Nusselt number, as described in equation (2):

$$Nu = h_{max} d_p / \lambda_g \quad (3)$$

Where h_{max} is defined as the maximum heat transfer coefficient and λ_g is the gas thermal conductivity. Borodulya et al. [102] have introduced a Nusselt number based on maximum conductive – convective heat transfer ($h_{pc} + h_{gc}$) which integrates also the Prandtl Number (*Pr*) and the Galileo Number (Ga).

Usually when we consider CFD models we see that the Ranz Marshal correlation [103] is used and applied:

$$Nu = 2.0 + 0.6 Re^{1/2} / Pr^{1/3} \quad (4)$$

Where Pr is the Prandtl number and it is equal to:

$$Pr = \mu c_g / \lambda_g \quad (5)$$

Where μ is the gas viscosity. Equation (5) is valid for dimensions of particles diameters from 100 μm to 4 mm and pressures comprised between atmospheric pressure and 10 MPa.

The conductive heat transfer is obviously proportional to the thermal conductivity of the particles and the contact area between particles.

Dealing with the final effect of pressure on the heat transfer: 0D models [104], CFD-DEM models [105] and experimental campaigns [106] show that on one hand the increase of pressure increases the heat transfer coefficients between wall to bed and between particles; on the other hand the amount of the increase is not linear. The implications of the improvements in the heat transfer which can be achieved with PCLC process are big, in fact from preliminary models developed in collaboration with Huazhong University of Science and Technology it seems that the improvement in heat transfer can counter balance the fact that the kinetics of the reduction reaction in the FR decreases its speed with the increase of pressure and could lead anyway to an increase of the reaction rate in pressurised conditions.

6. Designing Pressurised Chemical Looping combustors through 0D modeling and CFD modeling

The project GTCLC-NEG wants to define a clear approach in the design of PCLC reactors to be coupled with turbo expanders, to obtain the optimal power production efficiency. For this reason the main parameters to be analyzed are shown in Fig. 14 with the corresponding tool which is more adequate for the analysis and the design phase.

A possible strategy joining design with CFD together with ASPEN modeling and 0D-modeling is proposed in Fig. 14. In that sense this work can be considered as a first step in the development of the final power plant.

Given that Aspen modeling results have been dealt exhaustively in the section 2.1 of the paper, dealing with "Pressurised Chemical Looping: power plants layouts"; in the following sections the main work done in 0D-models development and CFD models development will be presented.

6.1. The importance of 0D models

Dealing with CLC reactor modeling approaches, a good amount of data is provided in the review of Adanez et al. 2012 [70] in which we see first of all the confirmation of the fact that most CLC plants are designed with the air reactor being a high velocity riser and the fuel reactor being a low velocity bubbling fluidised bed. We have to consider on the other hand that the fuel reactor can be operated also at velocities of the gaseous fuel which can be higher than that of the bubbling regime [107]. In Ref. [70] it is also underlined that the three main fields of analysis of the models of CLC reactors are basically:

- fluid dynamics,
- chemical reactions
- heat transfer.

For this reason, these aspects have been mentioned in the previous section.

If we focus our attention on macroscopic models, these can be used to have fast information on a first and less detailed design of the CLC reactors. In fact, these models allow the user already to have a good idea of the distribution of the gas between the emulsion and the bubbles and also of the distribution of the solids inside the bed, with low computational demands and in a short time. Particular attention has to be directed on the modeling of gas diffusion through the bed particles, in fact this represents a limiting phenomenon for the reduction reactions, which happen inside the fuel reactor. It is reported in Ref. [108] that without considering diffusion resistance between gases and solid particles the inventory which is necessary to carry out the reduction would be underestimated from 2 to 10 times. For this reason to describe the kinetics of the reacting oxygen carriers it is often used the Shrinking Core Model (SCM) [70], which takes into account efficiently all the processes that regulate the redox reactions of the oxygen carrier: the chemical reaction in the grain and the diffusion. Where the diffusion process can be divided into: diffusion into the film of gas which is surrounding the particle, diffusion into the pores and diffusion into the product layer around the grain (see Fig. 15).

Referring to the different mechanisms of diffusion, it can be also

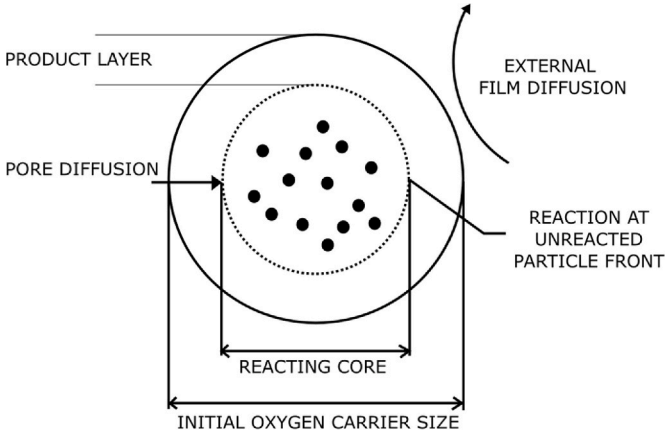

Fig. 15. Scheme of the Shrinking Core Model (SCM), adapted from [109].

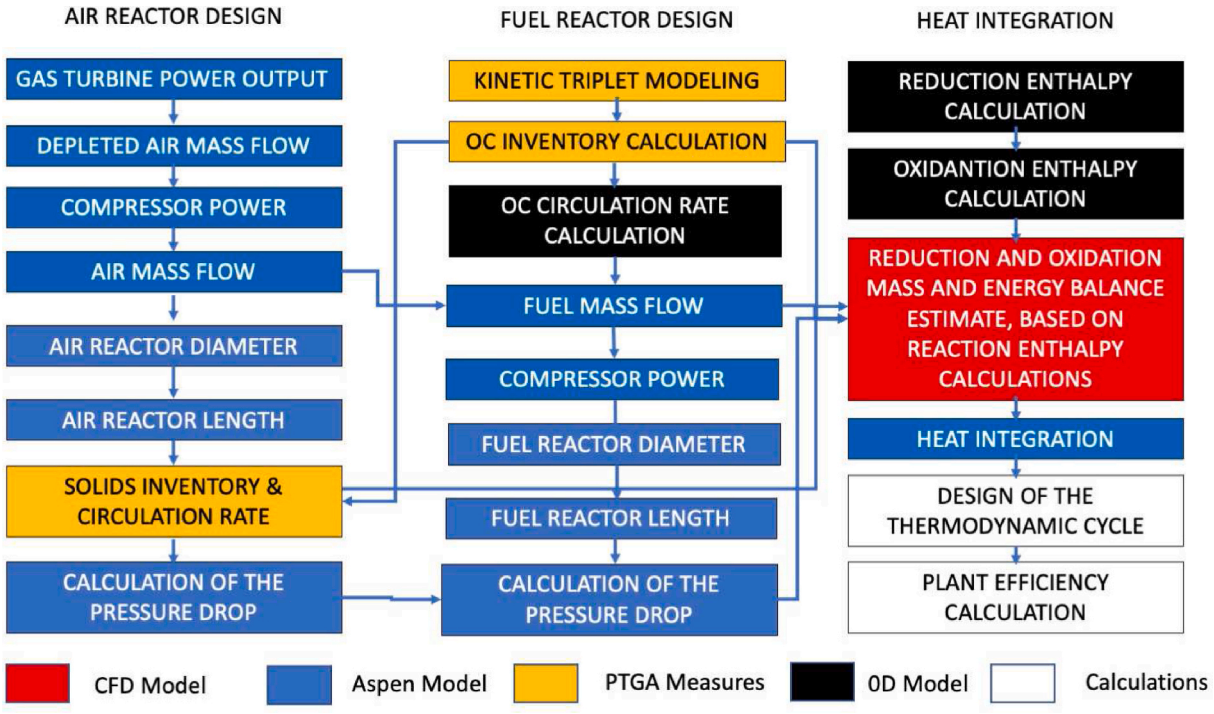

Fig. 14. GTCLC-NEG design approach.

considered in practical cases that the three types of diffusion can be aggregated into a product layer diffusion lumped term, see Ref. [110].

If we take into consideration the research work done in Refs. [111,112], the development of 0D or 1D models for the whole CLC reactor can be done taking into account the following aspects:

- fluid dynamics in the dense phase;
- fluid dynamics in the freeboard, mainly based on [113];
- mass balance in the reactor;
- mas balance in the dense bed;
- mass balance in the freeboard;
- oxygen carrier reactivity.

The model developed at CSIC, Instituto de Carboquimica, was calibrated with a CLC plant with a configuration shown in Fig. 16. It is interesting to note that in the layout shown in Fig. 16 both the air reactor and the fuel reactor are represented by bubbling fluidised beds. The fuel reactor is brought to the desired temperature with a furnace which provides heat also to compensate heat losses. Solids are moved from the fuel to the air reactor by making them pass through a loop seal (see (3), which is itself a small fluidised bed reactor). From the air reactor the oxidised oxygen carrier is transported through pneumatic transport (4) to a high-efficiency cyclone (5) and then stored in a solid reservoir (6) which prepares solids for a new cycle. The oxygen carrier used in the specific case shown in Fig. 16 is based on copper oxide.

Dealing with the fluid dynamics of the dense phase, this is modelled based on the approach of Johnsson et al. [114] which indicates that there are three main velocities to take into consideration:

1. the flow in the emulsion phase at the minimum fluidization velocity (u_{mf});
2. the visible bubble flow (u_{vis});
3. the gas throughflow (u_{tf}).

In this framework for the sake of modeling it is important also to consider the gas exchange between bubbles (which are related to the following velocities: u_{vis} and u_{tf}) and the emulsion (u_{mf}). At this point the Reynolds number under minimum fluidization conditions is calculated according to Ref. [115].

An interesting parameter which is also contained in Abad's model formulation [112] is the so-called "bubble fraction in the dense bed", which is expressed as:

$$\delta_b = u_{vis} / (u_{vis} + u_{b\infty}) \quad (6)$$

The parameter $u_{b\infty}$ reported in equation (6) is proposed in equation (7):

$$u_{b\infty} = 0.71\sqrt{g d_b} \quad (7)$$

where d_b is the bubble diameter. Based on the bubble fraction in the dense bed, the minimum fluidization porosity in the emulsion phase can be calculated.

The bubble diameter is also an important parameter, we can infer, and this gives us the possibility to connect the Abad's model with the work of Song et al. [116]. In synthesis the work of Song et al. [116] appears to be interesting because it is about the development of a new bubble based energy minimization multiscale method to analyze the difference between homogeneous and heterogeneous fluidization in pressurised conditions. In this work a bubble size correlation is derived from the experiments performed in a jetting fluidised bed. The final correlation obtained is the following:

This is an alternative correlation to that already presented by Cai [117]. The parameter d_b is the diameter of the bubble, H_d is the height reached by the bubble over the distributor; H_0 is a constant determined through experimental observation ($H_0 = 0.1$ when $H \leqq 0.09$ m and $H0 = 0.08$ when $H > 0.09$ m), P is the operating pressure, (U_g-U_{mf}) is the excess gas velocity, U_t^{Θ} and U_t are the terminal velocities of the particle respectively in ambient pressure conditions and elevated pressure conditions, U_j is jetting gas velocity and the constants $a = 0.0003$, $b = 0.25$, $c = 0.1$, $d = 3$.

Besides this approaches of significant importance is the one developed at Stanford University [118] in a Doctoral thesis, where a particle model is inserted in a system model, which with a similar approach to that adopted by Abad et al. [112] simulated: air reactor, fuel reactor, cyclones and the total CLC system. In that case the code is developed in Matlab instead of Fortran.

The implications of working with pressure in 0D modeling are many: from the implications on kinetics to the implications on bubble diameter (see equation (8)) and fluidization velocities to the implications on heat transfer. All of them have to be clearly modelled and calibrated against the real working environment.

6.2. CFD modeling approaches

CFD modeling approaches are based essentially on the Eulerian-Eulerian method and on the Eulerian-Lagrangian method. In the Eulerian-Eulerian method (also called two-fluid method, TFM), the different phases are treated as a continuum that runs through each other. The concept of phasic volume fraction is introduced for two phases and the sum of volume fractions is always 1. Volume fraction is a continuous function of time and space. A set of equations can be derived from the conservation equations of each phase, which have the same form for all phases. The equations can be closed by establishing some specific relations derived from the experimental data. For granular flows, the equations can be closed by applying the kinetic theory of molecules. The particle size and density of different particles as well as the movement trajectory of the particles are ignored for the description of the solid phase in the Eulerian-Eulerian method. Thus, the two fluids model has high calculation efficiency and has been widely used in the simulation of reactors from laboratory to pilot and full-scale plants [119,120]. Commercially available software, like ANSYS Fluent and open-source software like CFDlib, OpenFOAM and MFiX are all capable of performing Eulerian-Eulerian simulations. Similar forms of governing equations are solved in all of this software and the main difference between them is represented by the closures used for various sub models and by the numerical treatment [121]. A summary on FR CFD models developed up to 2021 is proposed in Table S1 of the supplementary material.

In the Eulerian-Lagrangian method, the gas phase is treated as the continuous phase and it is solved by Navier-Stokes equations. The discrete phase is obtained by calculating the movement of large number of particles in flow field. There can be an exchange of momentum, mass and energy between discrete phase and the gas phase. On the contrary of the Eulerian-Eulerian method, particle size, density and shape can be considered as parameters and particles can be tracked in time and space. One of the basic assumptions of the model is that the volume ratio of the discrete phase should be very low. Even so, large mass loading rates can still be analyzed. Particle trajectory calculation is independently performed. If the volume fractions are above 5%, the calculations are limited to the order of 2×105 particles [122]. To avoid this restriction, some methods have been developed to simplify the calculation, like the

$$d_b = 0.38(H_d + H_0)^{0.8} P^{0.06} (U_g - U_{mf})^{0.42} \left[U_t^{\Theta} / (2.56 U_t)\right] (U_j / U_t) \bullet \exp\left[-aP^2 - b(U_g - U_{mf})^2 - cP(U_g - U_{mf}) - d(Hd + H_0)(U_g - U_{mf})\right] \quad (8)$$

concept of parcel (which is used also in MP-PIC models). In the actual calculation process, several particles with same properties (species, temperature, size, etc.) are put into a parcel. Thus, limited parcels are tracked and this can greatly improve the calculation efficiency. It's worth to notice that, the size of parcels should be smaller than that of the smallest cell to avoid convergence problems (by avoiding that fluid volume fraction becomes 0).

CFD-DEM method has higher accuracy than the TFM method, but the calculation speed is slower. The whole process of collision or contact is solved by numerical integration of motion equations. Collisions are regarded as continuous processes occurring in finite time, in which the contact force is regarded as a continuous function of the distance between colliding particles [123]. Based on CFD-DEM, the DDPM model introduced the concept of parcels, to reduce computational costs. In DDPM, collisions between parcels are handled in two ways. One is the DDPM-DEM method, which considers the real collision process between particles. The other is the DDPM-KTGF method, which uses Kinetic Theory of Granular Flow (KTGF) to describe the interaction between particles to further decrease calculational costs. Therefore, the DDPM-DEM method is more similar to the CFD-DEM model than the DDPM-KTGF method [119].

FR mainly use gaseous fuels and solid fuels. Gaseous fuels have good reactivity because they are in the gas phase and can rapidly enter in contact with the oxygen carrier. Commonly used gaseous fuels are CH_4, H_2 and CO. A summary of recent studies on gaseous fuels is shown in Table 2S of the supplementary material.

The simulation of solid fuels is much more complex, because solid fuels enter in contact with the oxygen carrier and react in a more complex way, if compared to gaseous fuels. In the case of the fuel reactor fed with gaseous fuels, the oxygen carrier reduction is modelled based on the Shrinking Core Model (SCM) or the Nuclei Growth Model (NGM), see also [124]. The first models of fuel reactor fed with methane have been realised by Ref. [125]. Nickel is used in this case as an oxygen carrier. The parameters studied with these CFD models are mainly: gas-solid reaction rate, concentration of combustion exhaust gases and concentration of reactants. It was noted that the gas-solid reaction rate is usually higher in the emulsion phase, where the concentration of solids is higher. Then the reaction rate decreases along the height of the reactor. While the concentration of reactants and of product gases is oscillating in the dense phase (due to the passage of the bubbles), it becomes more stable in the freeboard where the solid is almost absent, see Ref. [126]. In Ref. [127] it was found that the increase of the superficial velocity lead to an increase in reactant concentration and a consequent decrease of the concentration of the gaseous products of the reduction reaction, because of the increase in bubble concentration and also in slagging. Two case studies, one on modeling the Internally Circulating Reactor (ICR) developed at NTNU and one on the results of the first modeling of the reactors used in the GTCLC-NEG project, are proposed in the supplementary material.

7. Guidelines and key design points for pressurised CLC combustors

In section 6 of this paper, which is about "Designing Pressurised Chemical Looping combustors through 0D modeling and CFD modeling", the key parameters to be optimised in the PCLC plant have been identified together with the software, which is needed for this task. In this section we apply the approach reported in Fig. 17, deriving the practical steps (or guidelines) to be followed in the design of the plant and showing also an example of the application of the guidelines, assuming that the plant is fed with syngas produced from biomass gasification (as an example).

7.1. Choosing the plant layout

The procedure presented in Fig. 17 sees as a first step, the

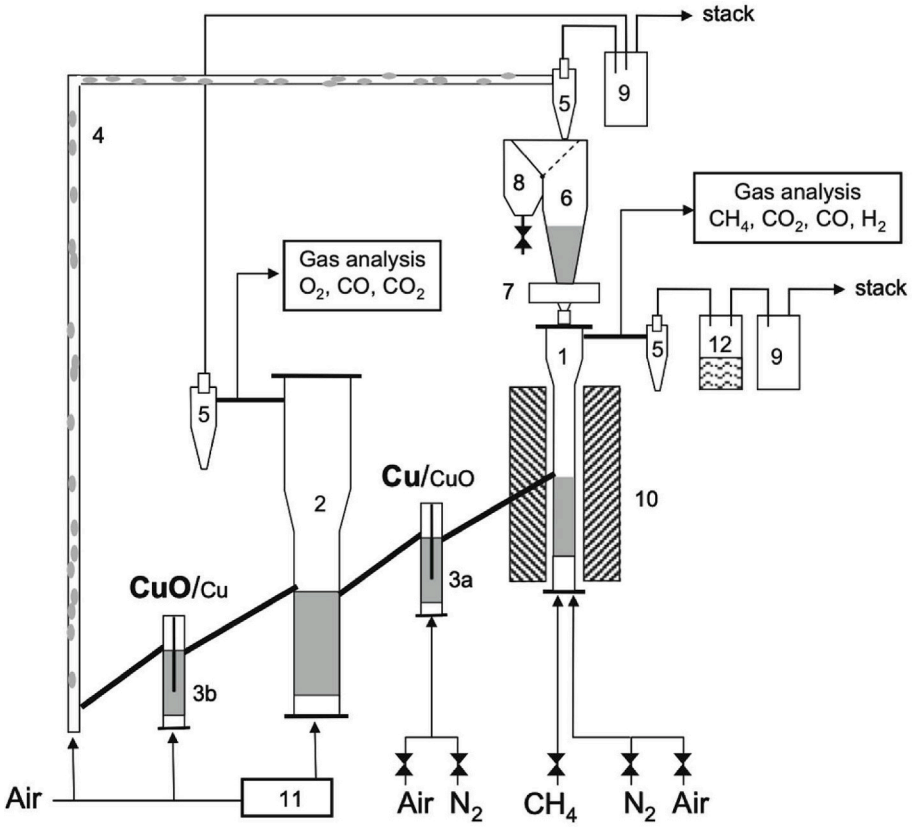

Fig. 16. Schematic diagram of the 10 kWth CLC prototype located at ICB-CSIC (Spain) [112].

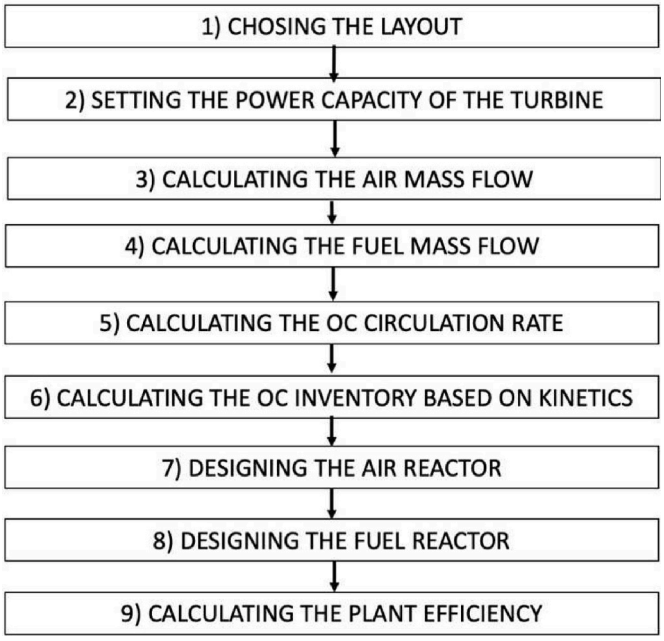

Fig. 17. Procedure for the design of the PCLC-based carbon negative emissions power plant.

identification of a certain plant layout. In this particular case the layout has been already shown in Fig. 1.

It is obviously based on the state of the art presented in paragraph 2 of this work and it is a configuration in which both: the depleted air coming from the air reactor and the exhaust gases exiting the fuel reactor expand in two separate turbo expanders. This is done to avoid mixing the gases coming from the air reactor and those coming from the fuel reactor and to grant a pure flow of CO_2 at the exit of the plant. The expanded gases (which have produced electrical power) are used then to recover heat in two HRSGs. It can be used also a single HRSG, but in this case two were chosen because we wanted to calculate the energy which is recovered separately by the air and by the fuel reactor.

7.2. Setting the power capacity of the turbine, the air mass flow and the fuel mass flow

If we assume a power of 12 MWe of the turbo expander, we can then model the plant in ASPEN Plus v11 (see Fig. 18) and calculate in detail:

- the air mass flow (which in this case it is equal to 135 t/h);
- the diameter and the length of the fluidised bed reactor, which is used as an air reactor and so it is configured as a riser.

The power capacity of 12 MWe is chosen because, working with biofuels the scale of the plant is limited by biomass availability and also because of the set of products offered on the market by main gas turbines producing companies.

7.3. Calculating the oxygen carrier circulation rate and the solids inventory

The circulation rate is calculated mainly based on a mass balance applied to the fuel reactor and depends on the conversion variation of the oxygen carrier, obtained in the fuel and air reactor.

Given that the flow of syngas is already known, we can calculate the circulation rate, according to equations (9) and (10), taken from

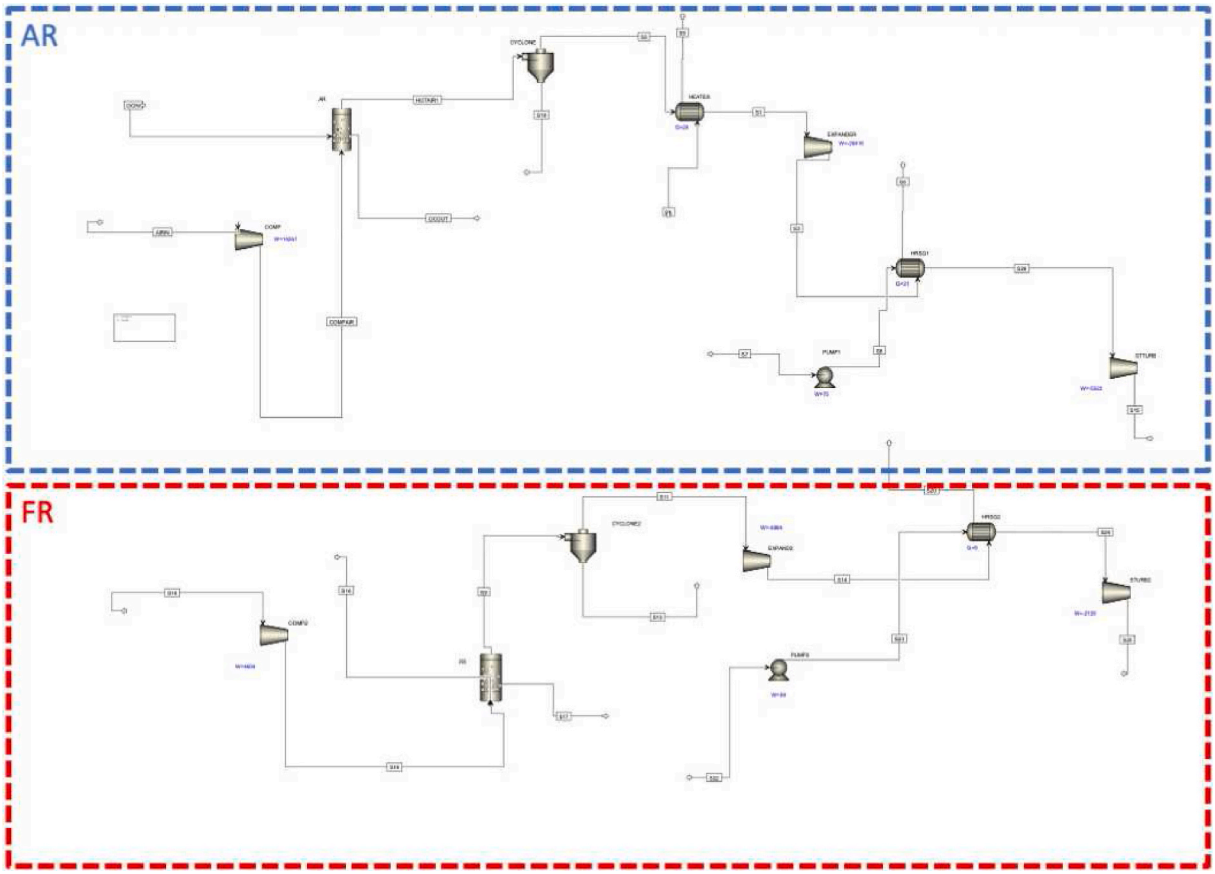

Fig. 18. Aspen Plus project of the air reactor (AR) and fuel reactor (FR).

Ref. [128].

$$\dot{m}_{ox} = b_r M_{NiO} F_f \Delta X_f / (x_{NiO} \Delta X_s) \quad (9)$$

$$\dot{m} = \dot{m}_{ox} (1 + R_0 x_{NiO} (X_{S,o} - 1)) \quad (10)$$

Where equation (9) represents the recirculation rate, expressed as the mass of oxygen carrier totally oxidised, while equation (10) is the real recirculation rate. The parameters shown in equations (9) and (10) are explained in the following paragraphs:

- b_r is the stoichiometric factor in the reduction reactions, expressed in mol of solid reacting per mol of fuel gas. In particular if we refer to the fuel reactor, we will have to consider the following reactions:

$$NiO + CO \rightarrow Ni + CO_2 \quad (11)$$

$$NiO + H_2 \rightarrow Ni + H_2O \quad (12)$$

In reality, if we use oxygen carriers based on nickel oxides, we have also to consider the water-gas-shift reaction.

- M is the molecular weight of the material, expressed in g per mole;
- F_f is the molar flow of the fuel gas, expressed in moles/s;
- ΔX_f is the conversion rate of the fuel gas, which is assumed to be equal to 1;
- x_{NiO} is the mass fraction of NiO in the fully oxidised sample; this parameter can be inferred directly from name of the oxygen carrier, for example if we take into consideration Ni40Al-FG: the two last letters mean freeze granulation, while the number 40 means 40% in mass of nickel metal is contained. This oxygen carrier has been tested in pressurised conditions at the Instituto de Carboquimica, see Ref. [78];
- ΔX_s represents the variation in the solids conversion. In fact not all the solids which are circulating in the reactor are fully converted, we can assume that 30% of the solids is converted, as reported for example in: [128].
- another key parameter of the oxygen carrier, after the mass fraction of metal, is the R_0, which is the oxygen transport capacity of the active metal oxide (for active metal oxide we indicate the part of the metal oxide which has not reacted with the support and so can actively behave as an oxygen carrier). These two data: mass fraction of metal oxide and oxygen transport capacity are indicated in Table 8 for Ni40Al-FG and are key parameters also for the design of the fuel and air reactor. R_0 can be calculated according to equation (13), as reported in Ref. [129];

$$R_0 = (m_{ox} - m_{red}) / m_{ox} \quad (13)$$

where m_{ox} and m_{red} are the masses of the oxidised and reduced form of the oxygen carrier, respectively.

- $X_{S,o}$ is the solids conversion in the oxidation reaction and can be calculated from equation (14).

$$X_{S,o} = 1 - \frac{m_{ox} - m}{m_{ox} R_0 x_{NiO}} \quad (14)$$

Where m is the mass of the sample. In reality in this case we assume that:

- in the air reactor the oxygen carrier enters with Xo = 0.5 and exits with Xo = 0.8;
- in the fuel reactor the oxygen carrier enters with Xr = 0.2 and exits with Xr = 0.5
- the variation in solids conversion rate for reduction (ΔX_r) and the variation in solids conversion rate for oxidation (ΔX_o) are both equal to 0.3.

Table 8
Ni40Al-FG Oxygen carrier characteristics [78].

Parameter	Value	Unit of measure
Active NiO content	40	wt%
Oxygen transport capacity	0.084	–
Particle size	0.2	(μm)
Porosity	0.36	%
Specific surface area (BET)	0.8	m2/g
Solid density	5380	kg/m3

The main characteristics of the oxygen carrier used are shown in Table 8.

As said before the oxygen carrier is derived from a freeze granulation preparation process, performed at Chalmers University, according to what reported in Ref. [130]. Based on equations (15) and (16) the final calculation of the circulation rate results to be equal to 111 kg/s, which is not excessive for a power plant producing 12 MWe and considering also other values reported in literature, see Ref. [128].

Also in the case of the solids inventory, this important design parameter is obtained from a mass balance performed at the air reactor and at the fuel reactor. So in this case we will have an optimal inventory for the air reactor and an optimal inventory of the fuel reactor. As already said these inventories will influence the bed height and the pressure drop so in the end also the pressure drop has to be checked to know if the two inventories are reasonable.

Based on a mass balance for both air reactor and fuel reactor the mass of oxygen carrier which is totally oxidised can be calculated based on the molar flow of the fuel gas [128]:

$$m_{ox,FR} = \frac{\rho_{NiO} b_r F_f}{x_{NiO} (-\bar{r}_{NiO})_r} \quad (15)$$

$$m_{ox,AR} = \frac{M_{NiO}}{M_{Ni}} \frac{\rho_{NiO} b_r F_f}{x_{NiO} (-\bar{r}_{Ni})_o} \quad (16)$$

Where:

- $m_{OX,FR}$ and $m_{OX,AR}$ are the inventory in the fuel reactor and in the air reactor, respectively.
- ρ_{NiO} is the density of the oxygen carrier, as reported in Table 8;
- $(-\bar{r}_{NiO})_r$ and $(-\bar{r}_{Ni})_o$ are the average reactions rate of the oxygen carrier per unit volume of the reacting solid, which can be calculated as explained in Ref. [128].

Equations (15) and (16) can be re-written in a simpler way, as also equation (17).

$$m_{OC} = y_g \Delta X_g \frac{2 d M_O}{R_0} \frac{\bar{\tau}_r}{\Phi_{FR}} \quad (17)$$

Equation (17) is for the determination of the solids inventory of the fuel reactor. For the determination of the inventory of the oxygen carrier in the air reactor we simply substitute the $\bar{\tau}_r$ and the Φ_{FR} with $\bar{\tau}_o$ and Φ_{AR}. Dealing with the other parameters, yg can be considered equal to 1, ΔX_g is equal to 0.999. While R_0 is a parameter which is typical of the oxygen carrier, d is typical of the reaction. In fact, d is the stoichiometric factor in the fuel combustion reaction with oxygen (expressed in mol O_2 per mol of fuel). Mo is the molar mass of oxygen (so it is 16). The expression: $\frac{2dM_O}{R_0}$ represents the characteristic circulation rate (also the enthalpy of reaction can be included in the expression at the denominator if we want to express the characteristic circulation rate based on the MW of primary energy of the reactor), also identified with the symbol: $\dot{m}_c$.

The parameter Φ_{FR} is the characteristic reactivity, which depends by the solid conversion at the inlet, $X_{r,in}$, and the variation of solids conversion ΔX_r, see Ref. [131].

The final inventory of the whole plant is given, obviously, by the sum of the inventory of the fuel reactor and that of the air reactor. If we have a fuel, like syngas, composed by two burning species (like H_2 and CO)

Table 9
Standard heat of reactions (ΔH_r^0) for the reduction and oxidation reactions of different oxygen carriers. Where the data are referred to 1 mole of gas or carbon and the units of measure are kJ/mol [70].

Redox system	ΔH_r^0 (kJ/mol gas or C)				
	CH_4	H_2	CO	C	O_2
CaSO4/CaS	158.6	−1.6	−42.7	86.9	−480.5
Co_3O_4/Co	107.9	−14.3	−55.4	61.6	−455.1
Co_3O_4/CoO	−16.8	−45.5	−86.6	−0.8	−392.7
CoO/Co	149.5	−3.9	−45.0	82.4	−475.9
CuO/Cu	−178.0	−85.8	−126.9	−81.4	−312.1
CuO/Cu_2O	−236.6	−100.4	−141.6	−110.7	−282.8
Cu_2O/Cu	−119.5	−71.1	−112.3	−52.1	−341.4
$CuAl_2O_4$/$CuAl_2O_3$	282.2	29.3	−11.8	148.7	−542.2
$CuAlO_2$/$CuAl_2O_3$	−24.1	−47.3	−88.4	−4.4	−389.1
$CuAl_2O_4$/$CuAlO_2$	588.5	105.9	64.7	301.9	−695.4
Fe_2O_3/Fe_3O_4	141.6	−5.8	−47.0	78.4	−472.0
Fe_2O_3/FeO	318.4	38.3	−2.8	166.8	−560.3
$Fe_2O_3Al_2O_3$/$FeAl_2O_4$	−62.3	−56.8	−98.0	−23.5	−370.0
Fe_2TiO_5/$FeTiO_3$	106.5	−14.6	−55.8	60.9	−454.4
Mn_2O_3/MnO	−48.0	−53.3	−94.4	−16.4	−377.1
Mn_2O_3/Mn_3O_4	−396.6	−140.4	−181.6	−190.7	−202.8
Mn_3O_4/MnO	126.3	−9.7	−50.8	70.8	−464.3
NiO/Ni	156.5	−2.1	−43.3	85.9	−479.4
$NiAl_2O_4$/$NiAl_2O_3$	158.6	−1.6	−42.8	86.9	−480.4

the inventory of the fuel reactor will be the sum oft he inventories which are necessary to oxidise hydrogen and carbon monoxide.

7.4. Designing the air reactor and the fuel reactor

Based on the plant realised in Aspen Plus v11, the design of the air reactor is performed, and we obtained a reactor with circular section and height of 9.5 meters and diameter of 2 meters due to the important amount of air which needs to flow through it (135 t/h). The air reactor is operated in a fast fluidization regime with a very small height of the bed bottom zone, while the height of the freeboard is important. Given the high mass flow the velocity is also high and this increases the elutriation index and the transport disengaging height. The pressure drop is about 0.5 bar. This value is also confirmed by some literature published on the topic, see Ref. [132]. This means that the influence of the pressure drop on the final plant efficiency is quite limited, while much more important is the influence of the inlet temperature of the air expanding in the turbo expander. This is assumed to be about 1300 °C at a pressure equal to 12 bar.

7.5. Calculating and optimised plant efficiency

The temperature of 1300 °C, at the exit of the air reactor, is based on the consideration that the enthalpy of reaction inside the air reactor is sufficient to heat up the incoming air and the circulating oxygen carrier. We have to consider in fact that the air, once it is compressed at 12 bar has already increased its enthalpy to 0.688 MJ/kg (as calculated by Aspen Plus V11). Knowing the enthalpy of the compressed air, we need to know then the enthalpy of the oxidation reaction, this data has been tabulated in Ref. [70] and are proposed in Table 9.

It is important noting from Table 9 that negative numbers of ΔH_r^0 indicate exothermic reactions, while positive numbers of ΔH_r^0 indicate endothermic reactions. Taking into account the data shown in the Table 9 and the data on the enthalpy of the compressed air fed to the air reactor (AR), the AR energy balance can be calculated with the following equation:

$$\begin{aligned} Q_{AR} = &\left[H^0_{MeO}{}^{*}m_{MeO} + m_{MeO}{}^{*}cp_{MeO}{}^{*}(T_{AR} - T_0)\right] \\ &- \lfloor \left(H^0_{Me}{}^{*}m_{Me}\right. \\ &\left. + m_{Me}{}^{*}cp_{Me}{}^{*}\left(T_{AR} - T_{FR}\right)\right) \\ &+ \left((m_{O2st}{}^{*}(alfa)^{*}cp_{O2}{}^{*}\left(T_{AR} - T_{comp}\right)\right) \\ &+ \left(m_{N2st}{}^{*}alfa^{*}cp_{N2}{}^{*}\left(T_{AR} - T_{comp}\right)\right)\rfloor + \mathrm{VR}^{*}\Delta P \end{aligned} \tag{18}$$

Where:

- Q_{AR} is the heat generated in the air reactor and then exchanged with the fuel reactor;
- H^0_{Me} is the enthalpy of formation of the metal in its reduced form; H^0_{MeO} is relative to the oxidised form;
- m_{Me} is the mass of the reduced metal; m_{MeO} is relative to the oxidised form;
- cp_{Me} is the specific heat of the reduced metal; cp_{Me} is relative to the oxidised form;
- T_{AR} is the temperature of the air reactor, which is set to be 1300 °C because it coincides with the turbine inlet temperature (TIT);
- T_0 is the standard temperature;
- T_{FR} is the temperature of the fuel reactor, which is set to be about 50 °C less than that of the Air Reactor, see Ref. [131];
- m_{O2st} is the mass of oxygen which reacts with the oxygen carrier oxidizing it;
- alfa is the ratio between the actual oxygen and the stoichiometric oxygen which reacts with the oxygen carrier; it represents the unknown in the equation;
- cp_{O2} is the specific heat of the oxygen;
- T_{comp} is the temperature at the exit of the compressor;
- m_{N2st} is the mass of the nitrogen contained in stoichiometric air;
- cp_{N2} is the specific heat of nitrogen;
- VR is the volume of the reactor;
- ΔP is the pressure loss, due to the bed height and the injection system as well.

Equation (18) has two unknowns: the heat which is provided at the fuel reactor by the oxygen carrier which circulates and so not only transports its mass from one reactor to another, but also transports energy in form of heat. The term indicated as Q_{AR} is the heat of the air reactor, which at equilibrium is equal to the heat adsorbed by the fuel reactor (if we assume that the losses are zero). For this reason, the excess air results to be the only unknown in a system of two equations. In this way iteratively we are able to determine what is the fuel mass flow, based on the optimal excess of air. Where the optimal excess of air is defined as the one which can still provide a temperature of the exiting gases which is set at about 1300 °C. Equation (19) is based on the difference between the enthalpy of the products and the enthalpy of the reagents of the reactions happening in the Fuel Reactor.

$$\begin{aligned} Q_{FR} = &\left[\left(H^0_{CO2}{}^{*}m_{CO2} + m_{CO2}{}^{*}cp_{CO2}{}^{*}(T_{FR} - T_0)\right) + \left(H^0_{H2O}{}^{*}m_{H2O} + m_{H2O}{}^{*}H_{H2O}\right) + \left(H^0_{Me}{}^{*}m_{Me} + m_{Me}{}^{*}cp_{Me}{}^{*}(T_{FR} - T_0)\right)\right] \\ &- \left[\left(H^0_{MeO}{}^{*}m_{MeO} + m_{MeO}{}^{*}cp_{MeO}{}^{*}\left(T_{FR} - T_{AR}\right)\right) + \left(H^0_{CO}{}^{*}m_{CO} + m_{CO}{}^{*}cp_{CO}{}^{*}\left(T_{FR} - T_{comp}\right) + \left(H^0_{H2}{}^{*}m_{H2} + m_{H2}{}^{*}cp_{H2}{}^{*}\left(T_{FR} - T_{comp}\right)\right]\right. + \mathrm{VR}^{*}\Delta P \end{aligned} \tag{19}$$

Where:

- Q_{FR} is the heat absorbed by the Fuel Reactor;
- H^0_{CO2} is the enthalpy of formation of CO_2;
- m_{CO2} is the mass of CO_2;

- cp_{CO2} is the specific heat of CO_2;
- H^0_{H2O} is the heat of formation of H_2O;
- m_{H2O} is the mass of water;
- H_{H2O} is the enthalpy o water, which takes into account: heating evaporation and further heating at the Fuel Reactor temperature;
- H^0CO and H^0H2 are respectively the enthalpies of formation of carbon monoxide and hydrogen;
- m_{CO} and m_{H2} are respectively the masses of carbon monoxide and hydrogen;
- cp_{CO} and cp_{H2} are respectively the specific heats of carbon monoxide and hydrogen.

8. Conclusions

This work, developed under the framework of the Marie Curie Project GTCLC-NEG, gives some guidelines and theoretical principles on the design of a Bioenergy with Carbon Capture and Storage plant based on the coupling of Chemical Looping Combustion with a turbo expander. A careful literature review has been made on the possible efficiencies, which can be gained with such a plant that represents a technological alternative to Natural Gast Combined Cycles with CCS. Usually this last type of plants can reach very high electrical efficiencies, but when they are coupled with carbon capture and storage they undergo an energy penalty, which can be comprised between 8–10%. After making a survey of the main layouts used to model plants working with pressurised chemical looping combustors to produce power, the paper describes which are the main reactor configurations, comparing the traditional setup of the chemical looping combustor (indicated as dual fluidised bed combustor or interconnected circulating fluidised beds) with two new reactor concepts:

- the Plug-flow Internally-circulating Reactor (PFIR) concept developed by Canmet ENERGY, Canada;
- the Internally Circulating Reactor (ICR) concept developed at NTNU, Norway.

Before introducing the advances in the modeling of such reactors some basic aspects on the influence of pressurised fluidization on reactor behavior are introduced. Pressure can have an important influence on:

- the hydrodynamics of the bed, generally the bubbles diameter decreases and the emulsion phase gets confounded with the bubble phase;
- the kinetics of the reduction reactions, which decreases, as denoted by many tests which have been performed on CH_4 and syngas;
- the attrition of the oxygen carrier particles, which increases;
- heat transfer, due to the change in density and viscosity of the gases moving inside the reactor.

For this reason, while new pilot plants of pressurised chemical looping combustion have been researched and developed, it is important to insert all the empirical relationships which we can detect with a Pressurised TGA into models which can describe the behavior of the reactor. CFD analysis already gives us some feedback on what could happen during the operation of such pilot plants. The fact that reduction and oxidation reactions appear to be mainly led by kinetics in PTGA tests does not imply that this behavior is always confirmed also at batch and pilot conditions. In those cases in fact we have to take into account also the heat transfer and the turbulence phenomena that happen in real reactors which can provide improvements in the fluidization phenomena and exchange of mass and heat and in a way counterbalance the decrease in reactivity revealed during pure kinetics measurements.

Finally after the state of the art on pressurised chemical looping combustion the paper presents some guidelines for designing pressurised fluidised bed combustors to be coupled with turbo expanders in carbon negative emissions power plants:

- the first step is to select the capacity of the desired turbine, based also on the biomass available in the territory where the project is developed;
- the second is to take into consideration the desired specifications of the turbine (like the turbine inlet temperature and the compression ratio);
- the third is to identify the mass flow of air;
- the fourth is to use a balance of energy applied to the fuel and air reactor to optimise the quantity of excess air reducing the use of fuel and granting high temperatures at the inlet of the turbine,
- the fifth is to identify in a recursive way the optimal quantity of fuel;
- the sixth is to calculate the oxygen carrier circulation rate;
- the seventh is to calculate the oxygen carrier inventory;
- the eighth is to calculate detailed mass and energy balances of the plant and so its efficiency.

Further steps will take into account the economic feasibility and optimization of such plants.

Declaration of competing interest

The authors declare that they have no known competing financial interests or personal relationships that could have appeared to influence the work reported in this paper.

Data availability

Data will be made available on request.

Acknowledgments

This work has been funded by the GTCLC-NEG project that has received funding from the European Union's Horizon 2020 Research and Innovation Programme under the Marie Sklodowska-Curie grant agreement No. 101018756. Special Acknowledgments are given to Dr. William A. Rogers of the National Energy Technology Laboratory (US) for helping in the concluding remarks on the arrangements needed to carefully model the effect of pressure on the PCLC plant.

Appendix A. Supplementary data

Supplementary data to this article can be found online at https://doi.org/10.1016/j.rser.2022.112851.

References

[1] Fridahl M, Lehtveer M. Bioenergy with carbon capture and storage (BECCS): global potential, investment preferences, and deployment barriers. Energy Res Social Sci 2018;42:155–65.
[2] Mendiara T, et al. Chemical looping combustion of biomass: an approach to BECCS. Energy Proc 2017;114:6021–9.
[3] Rydén M, et al. Negative CO2 emissions with chemical-looping combustion of biomass–a Nordic energy research flagship project. Energy Proc 2017;114:6074–82.
[4] Zhao X, et al. Biomass-based chemical looping technologies: the good, the bad and the future. Energy Environ Sci 2017;10(9):1885–910.
[5] Lyngfelt A, et al. 11,000 h of chemical-looping combustion operation—where are we and where do we want to go? Int J Greenh Gas Control 2019;88:38–56.
[6] Adánez J, et al. Chemical looping combustion of solid fuels. Prog Energy Combust Sci 2018;65:6–66.
[7] Mendiara T, et al. Negative CO2 emissions through the use of biofuels in chemical looping technology: a review. Appl Energy 2018;232:657–84.
[8] Bhui B, Vairakannu P. Prospects and issues of integration of co-combustion of solid fuels (coal and biomass) in chemical looping technology. J Environ Manag 2019;231:1241–56.
[9] Yu L, et al. Developing oxygen carriers for chemical looping biomass processing: challenges and opportunities. Adv Sustain Syst 2020;4(12):2000099.
[10] Osman M, et al. Review of pressurised chemical looping processes for power generation and chemical production with integrated CO2 capture. Fuel Process Technol 2021;214:106684.

[11] Kronberger B, et al. Design and fluid dynamic analysis of a bench−scale combustion system with CO2 separation− chemical−looping combustion. Ind Eng Chem Res 2005;44(3):546–56.
[12] Zerobin F, et al. Fluidised bed reactor design study for pressurised chemical looping combustion of natural gas. Powder Technol 2017;316:569–77.
[13] Wolf J, Anheden M, Yan J. Comparison of nickel-and iron-based oxygen carriers in chemical looping combustion for CO2 capture in power generation. Fuel 2005; 84(7–8):993–1006.
[14] Consonni S, et al. Chemical-looping combustion for combined cycles with CO 2 capture. J Eng Gas Turbines Power 2006;128(3):525–34.
[15] Barsali S, et al. Dynamic modelling of biomass power plant using micro gas turbine. Renew Energy 2015;80:806–18.
[16] Mattisson T, Lyngfelt A, Cho P. The use of iron oxide as an oxygen carrier in chemical-looping combustion of methane with inherent separation of CO2. Fuel 2001;80(13):1953–62.
[17] Chiesa P, et al. Three-reactors chemical looping process for hydrogen production. Int J Hydrogen Energy 2008;33(9):2233–45.
[18] Ishida M, Yamamoto M, Ohba T. Experimental results of chemical-looping combustion with NiO/NiAl2O4 particle circulation at 1200 C. Energy Convers Manag 2002;43(9–12):1469–78.
[19] Jin H, Ishida M. A novel gas turbine cycle with hydrogen-fueled chemical-looping combustion. Int J Hydrogen Energy 2000;25(12):1209–15.
[20] Porrazzo R, White G, Ocone R. Techno-economic investigation of a chemical looping combustion based power plant. Faraday Discuss 2016;192:437–57. 0.
[21] Wolf J, Anheden M, Yan J. Comparison of nickel- and iron-based oxygen carriers in chemical looping combustion for CO2 capture in power generation. Fuel 2005; 84(7):993–1006.
[22] Wolf J, Yan J. Parametric study of chemical looping combustion for tri-generation of hydrogen, heat, and electrical power with CO2 capture. Int J Energy Res 2005; 29(8):739–53.
[23] Iloeje CO, Zhao Z, Ghoniem AF. Design and techno-economic optimization of a rotary chemical looping combustion power plant with CO2 capture. Appl Energy 2018;231:1179–90.
[24] Petriz-Prieto MA, et al. A comparative simulation study of power generation plants involving chemical looping combustion systems. Comput Chem Eng 2016; 84:434–45.
[25] Zerobin F, Pröll T. Potential and limitations of power generation via chemical looping combustion of gaseous fuels. Int J Greenh Gas Control 2017;64:174–82.
[26] Khan MN, et al. Integration of chemical looping combustion for cost-effective CO2 capture from state-of-the-art natural gas combined cycles. Energy Convers Manag X 2020;7:100044.
[27] Oh D-H, Lee C-H, Lee J-C. Performance and cost analysis of natural gas combined cycle plants with chemical looping combustion. ACS Omega 2021;6(32): 21043–58.
[28] Naqvi R, Wolf J, Bolland O. Part-load analysis of a chemical looping combustion (CLC) combined cycle with CO2 capture. Energy 2007;32(4):360–70.
[29] Hughes R. Developments in fluidised bed conversion in Canada 2010-2015. Presentation; 2016.
[30] Cheng L, Basu P. Effect of pressure on loop seal operation for a pressurised circulating fluidised bed. Powder Technol 1999;103(3):203–11.
[31] Osman M. A pressurised Internally Circulating Reactor (ICR) for streamlining development of chemical looping technology. 2021.
[32] Adham K, CH, Kokourine A. Plug flow reactor with internal recirculation fluidised bed. 2015. CA2951724.
[33] Adham K, Harris C, Kokourine A. Modeling and process features of plug flow reactor with internal recirculation for biomass pyrolysis. J Chem Eng Process Technol 2017;8:353.
[34] Niass T, JK, Buchanan M, Svalestuen J, Park A, DePaolo D, Powel J. Accelerating breakthrough innovation in carbon capture. Huston, Texas: Utilization and Storage; 2017.
[35] McIntyre C. CPFD modeling of a novel internally circulating bubbling fluidised bed for chemical looping combustion. Université d'Ottawa/University of Ottawa; 2021.
[36] Cuenca MA, Anthony EJ. Pressurised fluidised bed combustion. Springer Science & Business Media; 2012.
[37] Llop MF, Casal J, Arnaldos J. Expansion of gas–solid fluidised beds at pressure and high temperature. Powder Technol 2000;107(3):212–25.
[38] Olowson P, Almstedt A-E. Influence of pressure and fluidization velocity on the bubble behaviour and gas flow distribution in a fluidised bed. Chem Eng Sci 1990; 45(7):1733–41.
[39] Olsson S, Wiman J, Almstedt A-E. Hydrodynamics of a pressurised fluidised bed with horizontal tubes: influence of pressure, fluidization velocity and tube-bank geometry. Chem Eng Sci 1995;50(4):581–92.
[40] Wiman J, Almstedt A-E. Hydrodynamics, erosion and heat transfer in a pressurised fluidised bed: influence of pressure, fluidization velocity, particle size and tube bank geometry. Chem Eng Sci 1997;52(16):2677–95.
[41] Wiman J, Almstedt A-E. Influence of pressure, fluidization velocity and particle size on the hydrodynamics of a freely bubbling fluidised bed. Chem Eng Sci 1998; 53(12):2167–76.
[42] Li J, Kuipers JAM. Effect of pressure on gas–solid flow behavior in dense gas-fluidised beds: a discrete particle simulation study. Powder Technol 2002;127(2): 173–84.
[43] Olowson P, Almstedt A-E. Hydrodynamics of a bubbling fluidised bed: influence of pressure and fluidization velocity in terms of drag force. Chem Eng Sci 1992;47 (2):357–66.
[44] Hoffmann A, Yates J. Experimental observations of fluidised beds at elevated pressures. Chem Eng Commun 1986;41(1–6):133–49.
[45] Rowe P, et al. X-ray observation of gas fluidised beds under pressure. Fluidization 1984;IV:53.
[46] Chan I, Sishtla C, Knowlton T. The effect of pressure on bubble parameters in gas-fluidised beds. Powder Technol 1987;53(3):217–35.
[47] Schweinzer J, Molerus O. Bubble flow in pressurised gas/solid fluidised beds. Chem Eng Technol 1987;10(1):368–75.
[48] Mansourpour Z, et al. Insights in hydrodynamics of bubbling fluidised beds at elevated pressure by DEM–CFD approach. Particuology 2010;8(5):407–14.
[49] Čárský M, et al. The bubble frequency in a fluidised bed at elevated pressure. Powder Technol 1990;61(3):251–4.
[50] Godlieb W, Deen N, Kuipers J. On the relationship between operating pressure and granular temperature: a discrete particle simulation study. Powder Technol 2008;182(2):250–6.
[51] Grace JR, Harrison D. The distribution of bubbles within a gas-fluidised bed. In: Inst. Chem. Eng. Symp. Ser., vol. 30; 1968. p. 105–25.
[52] Cai P. Effect of operating temperature and pressure on the transition from bubbling to turbulent fluidization. AICHE Symp Ser 1989;5(1):122–32.
[53] Canada G, McLaughlin M. Large particle fluidization and heat transfer at high pressures. AICHE Symp Ser 1978;74(176):27.
[54] Marzocchella A, Salatino P. The dynamics of fluidised beds under pressure. In: AIChE symposium series. American institute of chemical engineers; 1996.
[55] Marzocchella A, Salatino P. Fluidization of solids with CO2 at pressures from ambient to supercritical. AIChE J 2000;46(5):901–10.
[56] Yang W, Chitester D. Transition between bubbling and turbulent fluidization at elevated pressure. New York, NY: American Institute of Chemical Engineers; 1987.
[57] Chitester DC, et al. Characteristics of fluidization at high pressure. Chem Eng Sci 1984;39(2):253–61.
[58] Knowlton T. High-pressure fluidization characteristics of several particulate solids, primarily coal and coal-derived materials. AICHE Symp Ser 1977;3(161): 22–8.
[59] Li J, et al. Minimum and terminal velocity in fluidization of coal gasification materials and coal blending of gasification under pressure. Fuel 2013;110: 153–61.
[60] Chan I, Knowlton T. The effect of pressure on entrainment from bubbling gas-fluidised beds. In: Fluidization, Proc. 4th Int. Conf. on fluidization; 1984.
[61] Pemberton S, Davidson J. In: Kunii D, Toei R, editors. Elutriation of fine particles from bubbling fluidised beds. Fluidization. New York: Engineering Foundation; 1983. p. 275–82.
[62] Hirsan I, Sishtla C, Knowlton T. Effect of bed and jet parameters on vertical jet penetration length in gas fluidised beds. Chicago, IL (USA): Institute of Gas Technology; 1980 [Correlations].
[63] Knowlton TM. Pressure and temperature effects in fluid-particle systems. In: Fluidization, solids handling, and processing. Elsevier; 1999. p. 111–52.
[64] Shabanian J, Chaouki J. Effects of temperature, pressure, and interparticle forces on the hydrodynamics of a gas-solid fluidised bed. Chem Eng J 2017;313:580–90.
[65] Hedayati A, et al. Thermochemical conversion of biomass volatiles via chemical looping: comparison of ilmenite and steel converter waste materials as oxygen carriers. Fuel 2022;313:122638.
[66] Hedayati A, et al. Experimental evaluation of manganese ores for chemical looping conversion of synthetic biomass volatiles in a 300 W reactor system. J Environ Chem Eng 2021;9(2).
[67] Gogolev I, et al. Investigation of biomass alkali release in a dual circulating fluidised bed chemical looping combustion system. Fuel 2021;297:120743.
[68] Mei D, et al. Reactivity and lifetime assessment of an oxygen releasable manganese ore with biomass fuels in a 10 kWth pilot rig for chemical looping combustion. Fuel Process Technol 2021;215:106743.
[69] Gogolev I, et al. Commissioning, performance benchmarking, and investigation of alkali emissions in a 10 kWth solid fuel chemical looping combustion pilot. Fuel; 2021. p. 287.
[70] Adanez J, et al. Progress in chemical-looping combustion and reforming technologies. Prog Energy Combust Sci 2012;38(2):215–82.
[71] Kolbitsch P, et al. Comparison of two Ni-based oxygen carriers for chemical looping combustion of natural gas in 140 kW continuous looping operation. Ind Eng Chem Res 2009;48(11):5542–7.
[72] Pröll T, et al. Syngas and a separate nitrogen/argon stream via chemical looping reforming – a 140kW pilot plant study. Fuel 2010;89(6):1249–56.
[73] de Diego LF, et al. Bioethanol combustion with CO2 capture in a 1kWth Chemical Looping Combustion prototype: suitability of the oxygen carrier. Chem Eng J 2016;283:1405–13.
[74] Díez-Martín L, et al. Determination of the oxidation kinetics of high loaded CuO-based materials under suitable conditions for the Ca/Cu H2 production process. Fuel 2018;219:76–87.
[75] Rana S, et al. Ilmenite oxidation kinetics for pressurised chemical looping combustion of natural gas. Appl Energy 2019;238:747–59.
[76] García-Labiano F, et al. Effect of pressure on the behavior of copper-, iron-, and nickel-based oxygen carriers for chemical-looping combustion. Energy Fuels 2006;20(1):26–33.
[77] Bartocci P, et al. Integration of multiphase CFD models with detailed kinetics to understand the behavior of oxygen carriers under pressurised conditions. In: 13th international conference on applied energy (ICAE2021); 2021.
[78] Abad A, et al. Reduction kinetics of Cu-, Ni-, and Fe-based oxygen carriers using syngas (CO + H2) for chemical-looping combustion. Energy Fuels 2007;21(4): 1843–53.

[79] Siriwardane R, et al. Chemical-looping combustion of simulated synthesis gas using nickel oxide oxygen carrier supported on bentonite. Energy Fuels 2007;21(3):1582–91.
[80] Gu H, et al. Evaluation of the effect of sulfur on iron-ore oxygen carrier in chemical-looping combustion. Ind Eng Chem Res 2013;52(5):1795–805.
[81] Zhang S, Xiao R, Zheng W. Comparative study between fluidised-bed and fixed-bed operation modes in pressurised chemical looping combustion of coal. Appl Energy 2014;130:181–9.
[82] Xiao R, et al. Pressurised chemical-looping combustion of Chinese bituminous coal: cyclic performance and characterization of iron ore-based oxygen carrier. Energy Fuels 2010;24(2):1449–63.
[83] Xiao R, et al. Pressurised chemical-looping combustion of coal with an iron ore-based oxygen carrier. Combust Flame 2010;157(6):1140–53.
[84] Luo S, et al. Shale gas-to-syngas chemical looping process for stable shale gas conversion to high purity syngas with a H 2: CO ratio of 2: 1. Energy Environ Sci 2014;7(12):4104–17.
[85] Deshpande N, et al. High-pressure redox behavior of iron-oxide-based oxygen carriers for syngas generation from methane. Energy Fuels 2015;29(3):1469–78.
[86] Hamers H, et al. Reactivity of oxygen carriers for chemical-looping combustion in packed bed reactors under pressurised conditions. Energy Fuels 2015;29(4):2656–63.
[87] San Pio M, et al. Gas-solids kinetics of CuO/Al2O3 as an oxygen carrier for high-pressure chemical looping processes: the influence of the total pressure. Int J Hydrogen Energy 2017;42(17):12111–21.
[88] Lu X, et al. Pressurised chemical looping combustion with CO: reduction reactivity and oxygen-transport capacity of ilmenite ore. Appl Energy 2016;184:132–9.
[89] Tan Y, et al. Reduction kinetics of ilmenite ore for pressurised chemical looping combustion of simulated natural gas. Energy Fuels 2017;31(12):14201–10.
[90] Tan Y, et al. Reduction kinetics of ilmenite ore as an oxygen carrier for pressurised chemical looping combustion of methane. Energy Fuels 2017;31(7):7598–605.
[91] Chen L, et al. Experimental evaluations of solid-fueled pressurised chemical looping combustion–The effects of pressure, solid fuel and iron-based oxygen carriers. Appl Energy 2017;195:1012–22.
[92] Tian Q, Su Q. Performance of a Cu-based oxygen carrier with pressurised CH4 in a fixed bed CLC process. 2017.
[93] Lee D, et al. Experimental screening of oxygen carrier for a pressurised chemical looping combustion. Fuel Process Technol 2021;218:106860.
[94] Nordness O, et al. High-pressure chemical-looping of methane and synthesis gas with Ni and Cu oxygen carriers. Energy Fuels 2016;30(1):504–14.
[95] Guo X, et al. Reactivity of iron-based oxygen carriers with coal ash in pressurised chemical looping gasification. Fuel Process Technol 2021;219:106890.
[96] Garcia-Labiano F, et al. Effect of pressure on the behavior of copper-, iron-, and nickel-based oxygen carriers for chemical-looping combustion. Energy Fuels 2006;20(1):26–33.
[97] Sidorenko I, Rhodes MJ. Pressure effects on gas-solid fluidised bed behavior. Int J Chem React Eng 2003;1(1).
[98] Gogolek PEG, Grace JR. Fundamental hydrodynamics related to pressurised fluidised bed combustion. Prog Energy Combust Sci 1995;21(5):419–51.
[99] Botterill JSM, Desai M. Limiting factors in gas-fluidised bed heat transfer. Powder Technol 1972;6(4):231–8.
[100] Botterill JS. Fluid-bed heat transfer. Gas-fluidised bed behaviour and its influence on bed thermal properties. 1975.
[101] Molerus O, Wirth K-E. Heat transfer in fluidised beds, vol. 11. Springer Science & Business Media; 1997.
[102] Borodulya V, et al. Heat transfer between a surface and a fluidised bed: consideration of pressure and temperature effects. Int J Heat Mass Tran 1991;34(1):47–53.
[103] Ranz W. Evaporation from drops, parts I & II. Chem Eng Prog 1952;48:141–6.
[104] Di Natale F, Lancia A, Nigro R. A single particle model for surface-to-bed heat transfer in fluidised beds. Powder Technol 2008;187(1):68–78.
[105] Lian G, Zhong W, Liu X. Effects of gas composition and operating pressure on the heat transfer in an oxy-fuel fluidised bed: a CFD–DEM study. Chem Eng Sci 2022;249:117368.
[106] Looi AY, Mao Q-M, Rhodes M. Experimental study of pressurised gas-fluidised bed heat transfer. Int J Heat Mass Tran 2002;45(2):255–65.
[107] Kolbitsch P, et al. Comparison of two Ni-based oxygen carriers for chemical looping combustion of natural gas in 140 kW continuous looping operation. Ind Eng Chem Res 2009;48(11):5542–7.
[108] Abad A, et al. Modeling of the chemical-looping combustion of methane using a Cu-based oxygen-carrier. Combust Flame 2010;157(3):602–15.
[109] Deng Y, et al. Flue gas desulphurization in circulating fluidised beds. Energies 2019;12(20).
[110] Cabello A, et al. Kinetic determination of a highly reactive impregnated Fe2O3/Al2O3 oxygen carrier for use in gas-fueled chemical looping combustion. Chem Eng J 2014;258:265–80.
[111] Abad A, et al. Fuel reactor model validation: assessment of the key parameters affecting the chemical-looping combustion of coal. Int J Greenh Gas Control 2013;19:541–51.
[112] Abad A, et al. Modeling of the chemical-looping combustion of methane using a Cu-based oxygen-carrier. Combust Flame 2010;157(3):602–15.
[113] Kunii D, Levenspiel O. Fluidised reactor models. 1. For bubbling beds of fine, intermediate, and large particles. 2. For the lean phase: freeboard and fast fluidization. Ind Eng Chem Res 1990;29(7):1226–34.
[114] Johnsson F, Andersson S, Leckner B. Expansion of a freely bubbling fluidised bed. Powder Technol 1991;68(2):117–23.
[115] Wen C, Yu Y. A generalised method for predicting the minimum fluidization velocity. AIChE J 1966;12(3):610–2.
[116] Song S, et al. A bubble-based EMMS model for pressurised fluidization and its validation with data from a jetting fluidised bed. RSC Adv 2016;6(112):111041–51.
[117] Cai P, et al. Quantitative estimation of bubble size in PFBC. Powder Technol 1994;80(2):99–109.
[118] Goldstein EA. Modeling chemistry of copper-based oxygen carriers in chemical looping combustion systems. Stanford University; 2015.
[119] Shao Y, et al. Review of computational fluid dynamics studies on chemical looping combustion. J Energy Resour Technol Trans ASME 2021;143(8).
[120] Peng C, et al. Implementation of pseudo-turbulence closures in an Eulerian–Eulerian two-fluid model for non-isothermal gas–solid flow. Chem Eng Sci 2019;207:663–71.
[121] Garg R, et al. Open-source MFIX-DEM software for gas–solids flows: Part I—verification studies. 2012. p. 220.
[122] Ariyaratne WK, et al. CFD approaches for modeling gas-solids multiphase flows – a review. 2016.
[123] Namdarkedenji R, Hashemnia K, Emdad H. Effect of flow pulsation on fluidization degree of gas-solid fluidised beds by using coupled CFD-DEM. Adv Powder Technol 2018;29(12):3527–41.
[124] Kruggel-Emden H, Stepanek F, Munjiza A. A study on the role of reaction modeling in multi-phase CFD-based simulations of chemical looping combustion. Oil Gas Sci Technol Rev Energies Nouvelles 2011;66(2):313–31.
[125] Jung J, Gamwo IK. Multiphase CFD-based models for chemical looping combustion process: fuel reactor modeling. Powder Technol 2008;183(3):401–9.
[126] Wang X, et al. Three-dimensional simulation of a coal gas fueled chemical looping combustion process. Int J Greenh Gas Control 2011;5(6):1498–506.
[127] Mahalatkar K, et al. Computational fluid dynamic simulations of chemical looping fuel reactors utilizing gaseous fuels. Chem Eng Sci 2011;66(3):469–79.
[128] García-Labiano F, et al. Reduction and oxidation kinetics of a copper-based oxygen carrier prepared by impregnation for chemical-looping combustion. Ind Eng Chem Res 2004;43(26):8168–77.
[129] Dueso C, et al. Syngas combustion in a chemical-looping combustion system using an impregnated Ni-based oxygen carrier. Fuel 2009;88(12):2357–64.
[130] Cho P, Mattisson T, Lyngfelt A. Comparison of iron-, nickel-, copper- and manganese-based oxygen carriers for chemical-looping combustion. Fuel 2004;83(9):1215–25.
[131] Abad A, et al. Mapping of the range of operational conditions for Cu-, Fe-, and Ni-based oxygen carriers in chemical-looping combustion. Chem Eng Sci 2007;62(1–2):533–49.
[132] Khurram MS, et al. Relationship between solid flow rate and pressure drop in the riser of a pressurised circulating fluidised bed. J Chem Eng Jpn 2016;49(7):595–601.